**Pyruvate dehydrogenase kinase supports macrophage NLRP3 inflammasome activation during acute inflammation**

Allison K. Meyers[1], Zhan Wang[2, 10], Wenzheng Han[2, 3, 10], Qingxia Zhao[2, 10], Manal Zabalawi[2], Qianyi Zhang[4], Juan Liu[5], Rajesh K Manne[6], Felipe Lorenzo[7], Matthew A. Quinn[8], Qianqian Song[6], Daping Fan[9], Hui-Kuan Lin[6], Cristina M. Furdui[2], Jason W. Locasale[5], Charles E. McCall[1, 2], Xuewei Zhu[1, 2, 11, *]

[1.] Department of Microbiology and Immunology, Wake Forest School of Medicine, Winston-Salem, NC 27157, USA.

[2.] Department of Internal Medicine, Section on Molecular Medicine, Wake Forest School of Medicine, Winston-Salem, NC 27157, USA.

[3.] Department of Cardiology, Huadong Hospital Affiliated to Fudan University, Shanghai, 200040, China.

[4.] Department of Biology, Wake Forest University, Winston-Salem, NC 27109, USA.

[5.] Department of Pharmacology and Cancer Biology, Duke University School of Medicine, Durham, NC 27710, USA.

[6.] Department of Cancer Biology, Wake Forest School of Medicine, Winston-Salem, NC 27157, USA.

[7.] Department of Internal Medicine, Section on Endocrinology and Metabolism, Wake Forest School of Medicine, Winston-Salem, NC 27157, USA.

[8.] Department of Pathology, Wake Forest School of Medicine, Winston-Salem, NC 27157, USA.

[9.] Department of Cell Biology and Anatomy, University of South Carolina School of Medicine, Columbia, SC 29209, USA.

[10.] These authors contributed equally to this work.

[11.] Lead Contact.

* Correspondence: xwzhu@wakehealth.edu

**Summary**

Activating macrophage NLRP3 inflammasome can promote excessive inflammation, leading to severe cell and tissue damage and organ dysfunction. Here, we show that pharmacological or genetic inhibition of pyruvate dehydrogenase kinase (PDHK) significantly attenuates NLRP3 inflammasome activation in murine and human macrophages. PDHK inhibition lowers caspase-1 cleavage and IL-1β secretion in septic mice. PDHK inhibition reverses NLRP3 inflammasome-induced metabolic defect and enhances autophagic flux. Moreover, PDHK inhibition favors mitochondrial fusion over fission, attenuates mitochondrial ROS production, and preserves cristae ultrastructure. Unexpectedly, the suppressive effect of PDHK inhibition on the NLRP3 inflammasome is independent of pyruvate metabolism, pyruvate dehydrogenase, autophagy, or ROS production. In conclusion, our study suggests a non-canonical role for PDHK in supporting mitochondrial dysfunction and NLRP3 inflammasome activation during acute inflammation, independent of its canonical role as a pyruvate dehydrogenase regulator.

**Keywords**

NLRP3 inflammasome, macrophages, sepsis, pyruvate dehydrogenase kinase, immunometabolism, mitochondria, cristae, autophagy, mitochondrial fission and fusion

## Introduction

In sensing and promoting inflammation from diverse environmental threats, macrophages express pattern recognition receptors, including toll-like receptors (TLRs) and intracellular NOD-like receptors, such as NOD-, LRP-, and pyrin domain-containing protein 3 (NLRP3). Activation of NLRP3 results in assembly of the NLRP3 inflammasome, leading to self-cleavage of caspase-1, processing of IL-1β and IL-18, and pyroptotic cell death (pyroptosis) (Aachoui et al., 2013; Broz et al., 2012; Hagar et al., 2013; Kayagaki et al., 2011; Kayagaki et al., 2013; Rathinam et al., 2012). Macrophage NLRP3 inflammasomal response is critical for host defense against invading microbes (Broz et al., 2010; Fang et al., 2011). However, exaggerated NLRP3 inflammasome activation exacerbates tissue inflammation, cell death, and organ damage (Meyers and Zhu, 2020). Moreover, pyroptosis can reduce functional monocyte/macrophage numbers and activate the coagulation system by permitting the release of tissue factors (Wu et al., 2019). As a result, uncontrolled NLRP3 inflammasome activation accelerates the pathogenesis of many inflammatory diseases, including cardiovascular disease, type II diabetes, sepsis, and COVID-19 (Ferreira et al., 2021; Junqueira et al., 2022; Meyers and Zhu, 2020; Pan et al., 2021; Sefik et al., 2022). In light of these factors, uncovering new regulators of NLRP3 inflammasome activation may lead to novel therapeutic strategies for preventing and treating inflammatory diseases.

Mitochondria play a central role in NLRP3 inflammasome activation. Dysfunctional mitochondria release mitochondrial reactive oxygen species (mtROS) (Cruz et al., 2007; Zhou et al., 2011) and newly synthesized mitochondrial DNA (Nakahira et al., 2011; Shimada et al., 2012) or expose inner membrane cardiolipin on the outer membrane to activate the NLRP3 inflammasome (Iyer et al., 2013). Mitochondrial TCA cycle intermediates succinate (Mills et al., 2016; Tannahill et al., 2013), itaconate (Bambouskova et al., 2021; Hooftman et al., 2020; Swain et al., 2020), and fumarate (Humphries et al., 2020) differentially regulate NLRP3 inflammasome activation. Very recently, mitochondrial ATP instead of ROS has been proposed to activate the NLRP3 inflammasome (Billingham et al., 2022; Xian et al., 2021), complicating the role of mitochondria in regulating the NLRP3 inflammasome. Therefore, despite decades of research on the NLRP3 inflammasome, how macrophages reprogram cellular or mitochondrial metabolism to activate or inactivate the NLRP3 inflammasome is still not fully understood.

Mitochondrial pyruvate dehydrogenase (PDH) complex (PDC) is the gate-keeping and rate-limiting enzyme for mitochondrial glucose oxidation via decarboxylation of pyruvate to acetyl-CoA (Stacpoole, 2012). Pyruvate dehydrogenase kinase (PDHK isoforms 1-4) reversibly phosphorylates the PDHe1α subunit and inhibits PDC, whereas pyruvate dehydrogenase phosphatase (PDP) dephosphorylates and activates PDC (Karpova et al., 2003; Klyuyeva et al., 2019; Patel et al., 2014; Stacpoole, 2012). Interestingly, pyruvate dehydrogenase kinase 1 (PDHK1) is persistently expressed in monocytes and macrophages in septic mice and human blood monocytes (Liu et al., 2012). Targeting PDHK with its prototypic inhibitor dichloroacetate (DCA), a structural analog of pyruvate (the endogenous inhibitor of PDHK) (Stacpoole, 2012), protected mice against cecal-

ligation and puncture (CLP)-induced polymicrobial infection (McCall et al., 2018). However, the molecular mechanisms underlying DCA-induced septic protection and its relation to the regulation of the NLRP3 inflammasome are undefined.

Here, we demonstrate that pharmacological or genetic inhibition of PDHK *in vitro* suppresses macrophage NLRP3 inflammasome activation. PDHK inhibition also lowers caspase-1 cleavage and IL-1β secretion in septic mice. PDHK inhibition promotes macrophage metabolic and mitochondrial homeostasis during NLRP3 inflammasome activation. Unexpectedly, the suppressive effect of PDHK inhibition on the NLRP3 inflammasome is independent of pyruvate dehydrogenase, autophagy, or ROS production. Our study uncovers a non-canonical role for mitochondrial PDHK in supporting mitochondrial stress and NLRP3 inflammasome activation during acute inflammation.

## Results

### PDHK inhibition lowers macrophage NLRP3 inflammasome activation

To examine the effect of PDHK inhibition on macrophage NLRP3 inflammasome activation, we utilized two PDHK pharmacological inhibitors: DCA and JX06. The pan-PDHK inhibitor DCA blocks the four PDHK isoforms by binding to the pyruvate binding pocket of the kinase. In contrast, JX06 preferentially blocks PDHK isoform 1 by forming a disulfide bond with Cys240 in the ATP pocket of PDHK1 (Sun et al., 2015). Briefly, we treated murine bone marrow-derived macrophages (BMDMs) with DCA or JX06 for 30 min before LPS priming or after LPS priming by adding the inhibitors with the NLRP3 inflammasome inducers, including ATP, nigericin, and monosodium urate crystals (MSU), as depicted in **Figure 1A**. DCA or JX06 significantly reduced ATP, nigericin, or MSU-induced IL-1β secretion regardless of being added before or after LPS priming, except that DCA inhibited MSU-induced IL-1β secretion only when added after the LPS priming step (**Figures 1B-1C**). Interestingly, DCA or JX06 showed a more profound effect on IL-1β secretion when added after LPS priming (**Figures 1B-1C**). Therefore, in subsequent experiments, DCA or JX06 were added to the culture media after LPS priming unless specifically indicated. Moreover, DCA or JX06 dose-dependently suppressed ATP-induced IL-1β secretion (**Figures 1D-1E**), IL-1β cleavage (IL-1β p17), and caspase-1 cleavage (caspase-1 p20) (**Figures 1F-1G**). However, DCA or JX06 did not affect the intracellular protein level of inflammasome components (**Figures 1F-1G**). Consistently, DCA or JX06 showed a minor to no effect on the transcript expression of pro-IL-1β or NLRP3 when added before or after LPS priming (**Figures 1H-1I**). Additionally, DCA and JX06 induced a significant reduction in caspase-1 cleavage in macrophages treated with LPS plus nigericin (**Figures S1A-S1B**) or MSU (**Figures S1C-S1D**), respectively. Collectively, our results suggest that PDHK inhibition blocks macrophage NLRP3 inflammasome activation primarily by attenuating caspase-1 cleavage (Signal 2) but not LPS priming (Signal 1). Caspase-1 cleaves gasdermin D (GSDMD), leading to plasma membrane rupture, cell swelling (ballooning effect), and pyroptotic death (Chen et al., 2016; Kayagaki et al., 2015; Shi et al., 2015). PDHK inhibition prevented NLRP3-induced cellular swelling as indicated by decreased cellular area in DCA- or JX06-treated vs. LPS plus ATP-treated macrophages (**Figures S1E-S1F**). PDHK inhibition protected macrophages against LPS plus ATP-induced pyroptotic death, as shown by decreased propidium iodide (PI) or 7-amino-actinomycin D (7-AAD) staining (**Figures 1J-1K**) and less full-length and cleaved N-terminal GSDMD in the culture supernatant (**Figure 1L**). These results suggest that PDHK inhibition lowers macrophage NLRP3 inflammasome activation-induced inflammation and cell death. Both DCA and JX06 effectively inhibit NLRP3 inflammasome activation, suggesting that PDHK inhibition per se, rather than the particular binding site of the drug on the kinase (i.e., pyruvate binding pocket of PDHK for DCA vs. ATP pocket of PDHK for JX06), leads to the NLRP3 inflammasome inactivation.

In addition to murine macrophages, DCA and JX06 effectively lowered LPS plus ATP-induced IL-1β secretion and caspase-1 cleavage in human peripheral blood mononuclear cells (PBMCs)-derived macrophages (**Figures 1M-1N**), suggesting that PDHK inhibition can attenuate NLRP3 inflammasome activation in

macrophages regardless of the species. Interestingly, DCA or JX06 showed no effect on AIM2 inflammasome-mediated IL-1 production (**Figure S1G**). DCA had a minimal impact on LPS-induced non-inflammasome cytokine TNF or IL-6 secretion regardless of being added before or after LPS treatment (**Figures S1H-1I**). Unlike DCA, JX06 treatment moderately lowered LPS-induced TNF or IL-6 production (20% and 40% reduction, relative to the LPS group, respectively), when added before LPS stimulation (**Figures S1H-S1I**). These results suggest that PDHK inhibition has a more profound inhibitory effect on NLRP3 inflammasome-mediated inflammation.

**PDHK inhibition rewires cellular metabolism in NLRP3 inflammasome-activated macrophages**

We next assessed metabolic changes that occur with or without PDHK inhibition following NLRP3 inflammasome activation by high-resolution unbiased metabolomics analysis. A principal component analysis (PCA) of cellular metabolites (**Figure 2A**) demonstrated distinct segregation of each treatment group. Among the 236 metabolites detected, 101 metabolites (red) showed significant accumulation in the NLRP3 inflammasome-activated vs. control macrophages (**Figure 2B**). The top downregulated metabolites (green, n=93) in the inflammasome-activated vs. control macrophages were antioxidants (**Figure 2B**). Metabolite enrichment analysis revealed broad metabolic reprogramming in macrophages upon NLRP3 inflammasome activation (**Figure 2C**). Inhibition of PDHK by JX06 significantly altered 119 metabolites compared to inflammasome-activated macrophages (**Figure 2D**). Among them, bilirubin was one of the most up-regulated metabolites in JX06-treated macrophages compared to LPS plus ATP-treated cells. The pathway analysis of the metabolites demonstrated that the top regulated metabolic pathways with high pathway impact factors included porphyrin and chlorophyll metabolism, arachidonic acid metabolism, citrate cycle (TCA cycle), and pyruvate metabolism (**Figure 2E**). Collectively, these results indicate that PDHK inhibition by JX06 broadly influences cellular lipid, glucose, redox, and TCA cycle metabolism, demonstrating that PDHK is a vital kinase that controls macrophage metabolism under conditions of the NLRP3 inflammasome activation.

**PDHK inhibition promotes glycolysis in NLRP3 inflammasome-activated macrophages**

Pyruvate metabolism and PPP (**Figure 3A**) are two top metabolic pathways altered by JX06 treatment (**Figure 2E**). LPS plus ATP significantly increased glycolytic intermediate levels in macrophages, as measured by our untargeted metabolomics analysis (**Figure 3B)**. JX06 treatment further increased glycolytic intermediate accumulation except for intracellular lactate (**Figure 3B**). JX06 also increased the levels of PPP intermediates, including 6-phosphogluconate, sedoheptulose-7-phosphate, and erythrose-4-phosphate (**Figure 3C**). Given the metabolomics analysis only provides a snapshot of the concentrations of cellular metabolites, we next performed a Seahorse glycolysis stress test to further assess the effect of PDHK inhibition on glycolysis. LPS priming enhanced glycolysis and glycolysis capacity, as indicated by a significant increase in extracellular acidification rate (ECAR) after injection of glucose and oligomycin, respectively, relative to control (**Figures 3D-3E**). Interestingly, LPS plus ATP significantly lowered glycolysis and glycolysis capacity in those cells (**Figures**

**3D-3E**). DCA and JX06 both increased ECAR and restored glycolysis to the control level (**Figures 3D** and **3E**). Meanwhile, DCA but not JX06 restored the glycolytic capacity of the LPS+ATP-treated macrophages to the control level (**Figure 3E**). Note that DCA had no impact on glycolysis or glycolytic capacity in LPS-only treated macrophages (**Figure S2A-S2B**). To further investigate this, we examined macrophage glucose uptake using 2NBDG. Compared to control, LPS plus ATP treatment significantly impaired macrophage glucose uptake, while PDHK inhibition markedly reversed it (**Figure 3F**). Taken together, our data suggest that PDHK inhibition promotes glucose uptake and glycolysis in NLRP3 inflammasome-activated macrophages.

Given pyroptosis induces plasma membrane rupture and PDHK inhibition dampens pyroptotic cell death (**Figures 1J-1L**), we next examined the impact of pyroptosis on glycolytic metabolites using GSDMD-deficient macrophages by targeted metabolomics analysis. As expected, GSDMD-deficient macrophages showed a marked reduction in IL-1β secretion in response to LPS plus ATP stimulation (**Figure S2C**). Interestingly, PDHK inhibition by DCA or JX06 can still lower IL-1β secretion in GSDMD-deficient macrophages (**Figure S2C**). We did not observe a significant increase in glycolytic metabolites except for lactic acid in LPS-only treated macrophages in both wild-type (WT) and GSDMD-deficient macrophages (**Figure S2D**). Nevertheless, consistent with our untargeted metabolomics analysis results, LPS+ATP treated WT macrophages showed a higher abundance of the glycolytic metabolites compared to control. JX06 treatment further increased the concentrations of those metabolites in WT cells except for G6P/F6P (**Figure S2D**). We observed down-regulation of G6P/F6P but up-regulation of three other glycolytic metabolites (F1,6BP, 3PG/2PG, and PEP) in LSP plus ATP-treated GSDMD-deficient vs. WT macrophages (**Figure S2D**). These results suggest that pyroptosis alters glycolytic metabolite concentrations in NLRP3 inflammasome-activated macrophages but does not increase glycolytic metabolites universally. In response to JX06 treatment, GSDMD-deficient macrophages showed a significant increase in G3P/DHAP but only a trend toward an increase in 3PG/2PG and PEP (**Figure S2D**) relative to the WT counterparts. Collectively, our results suggest that macrophages reprogram glucose metabolism in response to the NLRP3 inflammasome activation and PDHK inhibition. The accumulation of glycolytic metabolites in the PDHK-inhibited macrophages is partially attributable to the improved cell membrane integrity.

**PDHK inhibition promotes mitochondrial respiration in NLRP3 inflammasome-activated macrophages**

We next assess whether mitochondrial glucose utilization increases as pyruvate can be oxidized to form acetyl-CoA to enter the TCA cycle via PDC (**Figure 3G**). Our untargeted metabolomics data showed that NLRP3 inflammasome activation by LPS+ATP significantly lowered TCA cycle intermediates, including citrate/isocitrate and cis-aconitate, but increased succinate relative to untreated control cells (**Figure 3H**). Concurrent with the changes to TCA cycle intermediates, NLRP3 inflammasome activation significantly lowered the levels of aspartate and alanine, a pyruvate carboxylase-dependent anaplerotic substrate (**Figure 3I**), and increased urea cycle intermediates such as ornithine and citrulline (**Figure 3I**). Interestingly, inhibition

of PDHK by JX06 in LPS plus ATP-treated macrophages elevated most of the TCA cycle intermediates (**Figure 3H**), increased aspartate and alanine, and elevated the levels of argininosuccinate, arginine, and citrulline (**Figure 3I**). These results suggest that PDHK inhibition altered activities of the TCA cycle and its coupled metabolic pathways, including malate-aspartate shuttle and aspartate-argininosuccinate shunt (**Figure 3G**), likely favoring TCA cycle intermediate replenishment for energy production.

Our Seahorse Mito Stress assay showed that LPS plus ATP treatment, but not LPS priming, significantly lowered basal respiration, maximal respiration, and ATP production-linked respiration, suggesting impaired mitochondrial respiration (**Figures 3J-3K**). PDHK inhibition markedly improved mitochondrial respiration in LPS plus ATP treated macrophages (**Figures 3J-3K**), but had no impact on mitochondrial respiration in LPS-only treated cells (**Figures S3A-S3B**). Additionally, LPS plus ATP treatment decreased total ATP production in macrophages, as quantified by the Seahorse XF real-time ATP rate assay (**Figure 3L**). PDHK inhibition by DCA rescued bioenergetic defects by elevating both glycolytic and mitochondrial ATP production (**Figure 3M**). A similar trend was seen in JX06-treated macrophages (**Figure 3M**). Taken together, our results suggest that PDHK inhibition supports mitochondrial fueling and restores macrophage metabolic and energy homeostasis following NLRP3 inflammasome activation.

Distinct from its changes in glycolytic metabolites, GSDMD deficiency showed a minor effect on the TCA cycle metabolites in LPS- or LPS plus ATP-treated macrophages (**Figure S3C**). JX06 also showed a minimal impact on the TCA cycle metabolites in LPS plus ATP-treated WT and Gsdmd$^{-/-}$ macrophages. The difference in the concentrations of the TCA cycle metabolites between our targeted and untargeted metabolomics analyses might be due to the different incubation times for JX06 and ATP in the two experiments (30 min vs. 45 min). Moreover, pretreating macrophages with glycine to block plasma membrane rupture showed no effect on mitochondrial respiration (**Figures S3D-S3E**). These data suggest that the metabolic changes in PDHK-inhibited macrophages are not solely attributable to the difference in plasma membrane integrity.

**PDHK inhibition-mediated NLRP3 inflammasome inactivation is independent of glucose metabolism or PDH**

To assess whether the enhanced glucose utilization accounts for PDHK inhibition-mediated NLRP3 inflammasome inactivation, we blocked glycolysis, PPP, and mitochondrial glucose metabolism by adding pharmacological inhibitors 30 min before ATP ± DCA stimulation (**Figure 4A**). Blockade of glycolysis using 2-DG (blocking hexose kinase), heptelidic acid (HA, blocking GAPDH), or sodium oxamate (blocking lactate dehydrogenase) at Signal 2 could not alter IL-1β secretion or reverse the inhibitory effects of DCA on IL-1β secretion (**Figure 4B**). Blockade of PPP by dehydroepiandrosterone (DHEA, blocking glucose-6-phosphate dehydrogenase) lowered LPS plus ATP-induced IL-1β secretion but could not reverse the effect of DCA on the inflammasome activation (**Figure 4C**). These data suggest that neither cytosolic glycolysis nor PPP

metabolism is attributable to attenuated ATP-induced IL-1β secretion in PDHK-inhibited macrophages. Next, blockade of mitochondrial pyruvate carrier by UK5099 (**Figure 4D**), PDH-dependent glucose oxidation by CPI-613 (also blocking α-ketogluconate dehydrogenase (α-KGDH) in the TCA cycle) (**Figure 4E**), or inhibition of PC-mediated pyruvate anaplerosis by chlorothricin (**Figure 4F**), suppressed ATP-induced IL-1β secretion, respectively, but had no impact on the inhibitory effect of DCA on ATP-induced IL-1β secretion. Additionally, blockade of other metabolic pathways that were altered by PDHK inhibition (**Figure S4A**), for example, the malate-aspartate shuttle by aminooxy acetic acid (AOAA) (**Figure S4B**) or aspartate-argininosuccinate shunt by fumonisin B1 (**Figure S4C**), could not restore IL-1β secretion. These results suggest that PDHK inhibition-mediated NLRP3 inflammasome inactivation does not directly result from enhanced glucose metabolism or other altered metabolic pathways coupled with the TCA cycle.

Our initial hypothesis is that PDHK inhibition promotes glucose/pyruvate oxidative metabolism by activating PDC in macrophages, leading to the inactivation of the NLRP3 inflammasome. For this hypothesis to be true, PDH inhibition should reverse the effect of DCA on NLRP3 inflammasome activation. To test this, we knocked down PDHe1α, the PDC subunit whose activity is negatively regulated by PDHK-mediated phosphorylation, using PDHe1α-specific siRNAs. PDHe1α transcript expression showed a 60% reduction in PDHe1α-silenced macrophages (**Figure 4G**). Silencing PDHe1α did not significantly alter the LPS plus ATP-induced IL-1β secretion (**Figure 4H**) but appeared to decrease caspase-1 cleavage (**Figure 4I**). Interestingly, DCA and JX06 still efficiently lowered LPS plus ATP-induced IL-1β production and caspase-1 cleavage in PDHe1α-silenced macrophages (**Figures 4H-4I**). Together, these data suggest that a) inhibition of PDH is unable to reverse the effect of PDHK inhibition on NLRP3 inflammasome activity; b) PDHK inhibition-mediated NLRP3 inflammasome inactivation does not result from PDH-induced glucose oxidation. To rule out the off-target effect of the PDHK inhibitors on the NLRP3 inflammasome, we knocked down the predominant macrophage PDHK isoforms to assess whether genetic inhibition of PDHK could mimic the effect of pharmacological inhibitors on NLRP3 inflammasome activity. PDHK1 showed the highest expression in macrophages among the four isoforms, whereas PDHK4 was the lowest abundant isoform at the transcript level (**Figure 4J**). NLRP3 inflammasome stimulation by LPS plus ATP lowered the transcriptional expression of PDHK isoforms 1 and 2, but not 3 or 4 (**Figure 4J**). Based on these results, we silenced the predominant macrophage PDHK isoforms 1 and 2. PDHK isoform-specific siRNAs effectively knocked down each isoform in macrophages (**Figure 4K**) and lowered LPS plus ATP-induced IL-1β secretion (**Figure 4L**). Moreover, silencing PDHK isoform 1, and to a much lesser extent, silencing isoforms 2, reduced LPS plus ATP-induced caspase-1 cleavage (**Figure 4M**), suggesting that genetic inhibition of PDHK also suppresses NLRP3 inflammasome activation. Collectively, our results indicate that PDHK regulates macrophage NLRP3 inflammasome activity by a mechanism independent of PDC-dependent glucose oxidation.

**PDHK inhibition promotes autophagic flux in NLRP3 inflammasome-activated macrophages**

Autophagy dampens NLRP3 inflammasome activation via multiple mechanisms, including clearance of assembled inflammasome complexes and removal of damaged mitochondria (Deretic, 2021; Kim et al., 2016). We next asked whether PDHK inhibition can promote autophagic flux in NLRP3 inflammasome-activated macrophages and if true, whether autophagy is responsible for the NLRP3 inflammasome inactivation in PDHK inhibited macrophages. In the absence of bafilomycin (blocking autophagosomal degradation in lysosomes), autophagy-associated protein LC3-II showed less expression in PDHK-inhibited macrophages compared to LPS plus ATP-treated cells. In contrast, in bafilomycin-treated macrophages, DCA or JX06 treatment enhanced the accumulation of both LC3-I and LC3-II (**Figure 5A**). PDHK inhibition also increased expression of the autophagic adaptor protein p62, which facilitates chaperon-mediated autophagy, of mitochondrial Tu translation elongation factor (TUFM), which specifically promotes mitophagy (autophagy of mitochondria) by interacting with Atg5-Atg12, Atg16L1 (Lei et al., 2012), or PINK1 (Lin et al., 2020), and of Parkin, which mediates mitophagy in a VDAC1 and p62-dependent manner (Geisler et al., 2010) (**Figure 5B**). These results suggest that PDHK inhibition promotes autophagy and mitophagy in inflammasome-activated macrophages. AMP kinase (AMPK) is an upstream regulator of autophagy and DCA activates AMPK in cardiac tissues (Li et al., 2019). We observed that NLRP3 inflammasome activation rapidly down-regulated phospho-AMPK (p-AMPK), total AMPK, and the ratio of p-AMPK/AMKP in macrophages (**Figures S5A-S5B**). However, DCA or JX06 did not significantly alter the ratio of p-AMPK/AMPK (**Figures S5A-S5B**). Blockade of AMPK by dorsomorphin had no impact on the on IL-1β secretion in PDHK-inhibited macrophages (**Figure S5C**), suggesting that the AMPK pathway does not contribute to NLRP3 inflammasome inactivation in those macrophages.

Next, we asked whether autophagy/mitophagy accounts for the attenuated NLRP3 inflammasome activation in PDHK-inhibited macrophages. We first used autophagy-deficient macrophages from myeloid cell-specific Atg5 KO mice. Atg5$^{-/-}$ macrophages showed a 95% reduction in atg5 transcript expression relative to control (**Figure 5C**) and had significantly less IL-1β secretion than control (**Figure 5D**), likely due to defective unconventional IL-1β secretion via the secretory autophagy machinery (Claude-Taupin et al., 2018; Dupont et al., 2011; Iula et al., 2018; Zhang et al., 2015). Interestingly, DCA and JX06 maintained their capacity to reduce IL-1β secretion (**Figure 5D**) and caspase-1 cleavage (**Figure 5E**) in atg5$^{-/-}$ macrophages. Similar results were obtained with 3-methyladenine (3-MA) to block autophagy (**Figure 5F**). Together, our data suggest that PDHK inhibition promotes autophagy/mitophagy activation under conditions of NLRP3 inflammasome activation. Autophagy is not required for decreased NLRP3 inflammasome activity in PDHK-inhibited macrophages.

**PDHK inhibition preserves mitochondrial structure and function in NLRP3 inflammasome-activated macrophages**

Mitochondria play a central role in the NLRP3 inflammasome (Misawa et al., 2013; Nakahira et al., 2011; Zhong et al., 2018; Zhou et al., 2011). As expected, activation of the NLRP3 inflammasome by LPS plus ATP

triggered a robust mtROS production (**Figure 6A**). PDHK inhibition by DCA or JX06 led to a 50% reduction in mtROS production (**Figure 6A**). Consistently, LPS plus ATP treatment depleted the metabolites in the methionine-cysteine-glutathione pathways (**Figure S6A**) and $NAD^+$ biosynthetic metabolites (**Figure S6B**), reflecting an excessive oxidative stress condition, which was partially restored by JX06 treatment (**Figure S6B**). Together, our data suggest that PDHK inhibition protects macrophages against oxidative stress, particularly mitochondrial oxidative stress. We next imaged mitochondria in macrophages stained with MitoTracker Deep Red FM using confocal microscopy. In response to NLRP3 inflammasome stimulation, mitochondria underwent a morphological change from a string-like shape to a dot-like shape (**Figure 6B**), consistent with previous reports (Misawa et al., 2015; Misawa et al., 2013). PDHK inhibition by DCA or JX06 maintained mitochondria in a more string-like shape (**Figure 6B**). Further, morphometric analysis of transmission electron microscopy images (**Figure 6C**) revealed a significant reduction in both mitochondrial length and perimeter in LPS plus ATP-treated vs. control macrophages (**Figures 6D-6E**), suggesting increased mitochondrial fragmentation. PDHK inhibition partially abolished mitochondrial fragmentation, as evidenced by greater mitochondrial length and perimeter in DCA or JX06-treated macrophages (**Figures 6D-6E**). However, PDHK inhibition did not alter the mitochondrial number, aspect ratio (major axis/minor axis), or roundness compared to NLRP3 inflammasome activation (**Figure S6C**). Moreover, LPS plus ATP treatment reduced cristae number per mitochondrion (**Figures 6F-6G**) and increased cristae widening (**Figures 6F and 6H)**. Interestingly, PDHK inhibition partially restored cristae density and narrowed cristae (**Figures 6F and 6H**). Because cristae shape governs mitochondrial respiration and stacking cristae supports mitochondrial bioenergetics (Cogliati et al., 2013), our data suggest that inhibition of PDHK improves mitochondrial functionality and repurposes mitochondria toward oxidative respiration by preserving mitochondrial morphology and cristae ultrastructure.

Mitochondria are dynamic organelles undergoing continual fusion and fission, a process regulated by a family of dynamin-related GTPases, including mitochondrial fission protein dynamin-related protein 1 (Drp1) (Cereghetti et al., 2008; Smirnova et al., 2001) and fusion protein optic atrophy protein 1 (OPA1) (Mishra et al., 2014). Consistent with the increased mitochondrial fragmentation, the protein level of p-Drp1 (Ser616) was markedly increased at 30 min post ATP treatment and its level reduced to the baseline at 60 or 120 min ATP treatment (**Figure 6I**). The OPA1 level remained low during 60 min ATP exposure and slightly increased at 120 min ATP stimulation (**Figure 6I**). Interestingly, PDHK inhibition by DCA attenuated ATP-induced phospho-Drp1 (Ser616) expression and increased OPA1 protein level (**Figure 6I**). Notably, genetic deletion of PDHK1 increased OPA1 transcript and protein expression at the basal state and after 1 h ATP stimulation (**Figures 6J-6K**). Not surprisingly, p-Drp1 (Ser616) expression did not differ between genotypes, given that its expression declined after 1 h ATP stimulation (**Figure 6K**). Together, our data suggest that PDHK inhibition promotes mitochondrial fusion and preserves cristae ultrastructure to support mitochondrial fitness during acute inflammation.

**PDHK inhibition-mediated NLRP3 inflammasome inactivation is independent of mitochondrial fusion or mitochondrial ROS**

Mitochondrial elongation promotes NLRP3 inflammasome in an ERK1/2-dependent manner (Park et al., 2015). Mitochondrial fusion is also implicated in preventing NLRP3 inflammasome activation (Pereira et al., 2022).To examine the role of mitochondrial fusion or OPA1 expression on PDHK-regulated inflammasome activity, we inhibited OPA1 in macrophages using a pharmacological inhibitor or siRNAs. When added together with ATP and DCA, MYLS22, a selective OPA1 inhibitor, partially abolished the suppressive effect of DCA on IL-1β secretion (**Figure S6D**). When added 30 min before LPS priming, MYLS22 could not restore IL-1β secretion (**Figure S6E**), suggesting that the reversal effect of MYLS22 acts primarily on Signal 2. OPA1 siRNAs sufficiently knocked down OPA1 protein expression in macrophages (**Figure 6L**). However, they could not restore IL-1β secretion in DCA-treated cells (**Figure 6M, Figure S7F**), suggesting that OPA1 protein expression is not required for PDHK inhibition-mediated NLRP3 inflammasome inactivation. The differential effects of OPA1 inhibition by MYLS22 and siRNAs may result from their different impact on mitochondrial dynamics following NLRP3 inflammasome activation. We also do not rule out the off-target effect of MYLS22 in our experiment. Early ERK1/2 activation promotes DRP1-dependent mitochondrial fission (Prieto et al., 2016). Concomitant with rapidly increased DRP1 phosphorylation, we observed LPS plus ATP rapidly activated ERK1/2 at 15 min post ATP stimulation, whereas DCA attenuated ERK1/2 phosphorylation at 15 min (**Figures S6G-S6H**). However, blockade of ERK by U0126 did not affect the inhibitory effect of DCA on IL-1β secretion (**Figure S6I**).

Lastly, to assess whether PDHK inhibition-mediated NLRP3 inflammasome inactivation results from attenuated mtROS, we stimulate mtROS production by using mitoParaquat (MitoPQ). MitoPQ at 10 or 50 μM increased mtROS production in macrophages treated with or without DCA compared to their counterparts (**Figure 6N**). 50 μM MitoPQ also significantly increased IL-1β secretion in LPS plus ATP-treated macrophages (**Figure 6O**). Interestingly, DCA equally lowered IL-1β secretion to the same level in macrophages treated with and without MitoPQ (Figure 6O). Collectively, our results suggest that down-regulation of mitochondrial ROS production is not required for PDHK inhibition-mediated NLRP3 inflammasome inactivation.

**PDHK inhibition lowers plasma IL-1β and blood monocyte caspase-1 activity in septic mice**

Previous studies of murine sepsis demonstrate that *in vivo* targeting of PDHK with DCA, administered as a single dose of 25 mg/kg 24 h post CLP, increases the septic survival rate to 71%, whereas the CLP animals not receiving DCA treatment had a survival rate of only 10% over the 14-day observation period (McCall et al., 2018). Despite the less effect of PDHK inhibition on LPS-induced cytokine expression in BMDMs (**Figures S1H-S1I**), very recently, our group demonstrated that *in vivo* PDHK inhibition by DCA lowered plasma non-inflammasome cytokines, including TNF and IL-6 in the CLP mice (Oh et al., 2022), suggesting an anti-inflammatory effect of PDHK inhibitors in bacteria-infected animals. Given that macrophage NLRP3

inflammasome plays a critical role in the pathogenesis of sepsis, we asked whether DCA confers survival partially through down-regulation of the NLRP3 inflammasome during sepsis. To test this, we first analyzed the concentrations of plasma IL-1β and IL-18. DCA (25 mg/kg) was given to septic mice 24 h post CLP for 6 h (**Figure 7A**)**.** CLP-induced septic mice showed significantly elevated plasma IL-1β and IL-18 concentrations relative to sham control (**Figures 7B-7C**). To examine pyroptosis, we measured the concentrations of plasma lactate dehydrogenase (LDH, a cell death marker) and cleaved N-terminal (NT) GSDMD. At 30 h post-CLP, plasma NT-GSDMD was undetectable, and there was a trend toward an increase in plasma LDH in CLP vs. control mice (**Figure 7D**). CLP mice displayed a higher percentage of monocytes (identified as $CD115^{+}Ly6G^{-}$) and neutrophils ($CD115^{-}Ly6G^{+}$) (**Figures 7E-7G**) in peripheral blood circulation, indicating monocytosis and neutrophilia, respectively. Moreover, we observed a more than 3-fold increase in FLICA (FAM-YVAD-FMK) staining in blood monocytes ($CD115^{+}Ly6G^{-}$) and a 2-fold increase in FLICA staining in neutrophils ($CD115^{-}Ly6G^{+}$) (**Figures 7H-7K**), suggesting elevated caspase-1 cleavage in blood myeloid cells in the CLP vs. sham control mice. Interestingly, DCA treatment significantly decreased plasma IL-1β (**Figure 7B**), lowered plasma LDH (**Figure 7D**), and reduced caspase-1 cleavage in both blood monocytes and neutrophils (**Figures 7H-7K**). It also tended to decrease plasma IL-18 (**Figure 7C**). Because IL-1β drives neutrophil recruitment and DCA lowered plasma IL-1β, not surprisingly, DCA treatment prevented neutrophilia but not monocytosis in CLP mice (**Figures 7E-7G**). Collectively, our data suggest that inhibition of PDHK attenuates inflammasome-triggered caspase-1 activation and cytokine production during sepsis *in vivo*, which may partially contribute to the decreased septic mortality in DCA injected mice.

## Discussion

Macrophage NLRP3 inflammasome has emerged as a crucial driver of sepsis-associated inflammation (Danielski et al., 2020). PDHK is a mitochondrial metabolic regulator that dictates the activity of the PDC. By phosphorylating the PDHe1α subunit of PDC, PDHK effectively blocks the conversion of pyruvate into acetyl-CoA such that pyruvate can no longer be utilized by the mitochondria in the TCA cycle. Pharmacologically targeting PDHK with a pan-PDHK inhibitor DCA enhances septic mouse survival (McCall et al., 2018) and rebalances metabolic dysregulation in septic mouse liver (Mainali et al., 2021) or inflammatory THP1 monocytes (Zhu et al., 2020). Here, our *in vivo* study demonstrates that DCA lowers circulating IL-1β and LDH concentrations, attenuates blood neutrophilia, and reduces caspase-1 activities in blood myeloid cells in septic mice, suggesting that PDHK promotes NLRP3 inflammasome activation during sepsis. Our *in vitro* study confirms the role of mitochondrial PDHK in supporting NLRP3 inflammasome activation in murine and human macrophages, occurring independently of PDH-dependent pyruvate oxidation. Moreover, we uncover that PDHK promotes mitochondrial oxidative damage and fragmentation and impairs cristae integrity, supporting NLRP3 inflammasome-induced inflammation and pyroptotic cell death.

PDHK inhibition markedly reduced NLRP3 inflammasome activation but had a minimal effect on LPS-induced IL-1β, NLRP3, TNF expression, or AIM 2 inflammasome activation, suggesting a pathway-specific effect of PDHK on macrophage inflammation. We initially hypothesized that PDHK supports NLRP3 inflammasome activation by downregulating PDH-dependent pyruvate metabolism. If this hypothesis were true, inhibition of PDH or mitochondrial pyruvate utilization would counteract the DCA effect on inflammasome activation. Interestingly, blockade of pyruvate transport into mitochondria, inhibition of PC-dependent pyruvate anaplerosis, or inhibition of PDH-dependent pyruvate oxidation at Signal 2 all markedly reduced IL-1β secretion. Consistent with our findings, mitochondrial pyruvate-derived citrate is transported into the cytosol for fatty acid synthesis to support the NLRP3 inflammasome activation (Moon et al., 2015). PDH-dependent pyruvate flux enhances LPS-induced macrophage inflammation (Meiser et al., 2016). Thus, our results and other published work suggest that mitochondrial pyruvate metabolism is required for NLRP3 inflammasome activation. Notably, inhibition of mitochondrial pyruvate metabolism could not reverse the suppressive effect of DCA on inflammasome activation. Moreover, both DCA and JX06 effectively lowered IL-1β secretion in PDHe1α-silenced macrophages. Our findings suggest a novel role for PDHK in regulating the NLRP3 inflammasome, independent of phosphorylation of PDH for pyruvate oxidation.

Mitochondrial dysfunction drives NLRP3 inflammasome activation. Our results clearly showed that PDHK inhibition protects macrophages against NLRP3 inflammasome activation-induced mitochondrial oxidative damage and dysfunction, as evidenced by 1) reduced mitochondrial fragmentation, 2) preserved cristae ultrastructure, 3) attenuated mtROS production, and 4) enhanced ATP generation. Intriguingly, a recent study reported that mitochondrial electron transport chain (ETC)-generated ATP, but not ROS, is required for

activating NLRP3 inflammasome (Billingham et al., 2022). In our study, down-regulation of mtROS is not necessary for PDHK inhibition-mediated NLRP3 inflammasome inactivation, given that DCA can equally lower LPS plus ATP-induced IL-1β secretion in macrophages treated with or without mitoPQ. Moreover, because PDHK inhibition enhances glycolysis, mitochondrial respiration, and total ATP production in NLRP3-activated macrophages, it is unlikely that the down-regulation of NLRP3 inflammasome activation in PDHK-inhibited cells results from decreased mitochondrial ETC activities. Controversial results exist regarding the role of mitochondrial dynamics in macrophage NLRP3 inflammasome activation (Ichinohe et al., 2013; Park et al., 2015; Pereira et al., 2022). In our study, PDHK-inhibited macrophages displayed decreased mitochondrial fission protein p-DRP1 and conversely increased mitochondrial fusion protein OPA1 expression, in parallel with the improved mitochondrial morphology and cristae ultrastructure, under conditions of NLRP3 inflammasome activation. However, knockdown of OPA1 or indirect inhibition of Drp-mediated mitochondrial fission by blockade of ERK1/2 signaling pathway could not reverse the effect of DCA on NLRP3 inflammasome activation, suggesting that PDHK inhibition-mediated NLRP3 inflammasome inactivation is independent of OPA1 expression or mitochondrial elongation.

At the later stage of human sepsis, leukocytes display a generalized metabolic defect (Cheng et al., 2016). Interestingly, LPS-primed macrophages showed elevated Warburg glycolysis and unaltered mitochondrial respiration, mimicking the initial step of sepsis (Cheng et al., 2016). LPS plus ATP-induced NLRP3 inflammasome activation parallels broad metabolic defect in macrophages, mimicking the metabolic paralysis at the late stage of sepsis. PDHK inhibition at Signal 2 broadly rewired cellular metabolic pathways and rescued metabolic defects by increasing glucose uptake, glycolysis, and mitochondrial respiration. Intriguingly, PDHK inhibition promotes mitochondrial fusion over fission and protects mitochondrial cristae ultrastructure to support mitochondrial fitness. Mitochondrial cristae shape regulates respiratory chain super-complex stability and assembly (Cogliati et al., 2013). Although mitochondrial dynamics has no impact on PDHK-regulated NLRP3 inflammasome activity, our results suggest a role for PDHK in supporting mitochondrial oxidative stress/damage, mitochondrial fission over fusion, and cristae remodeling upon NLRP3 inflammasome stimulation. The underlying mechanisms of mitochondrial structural retrieval by PDHK inhibition are unknown and require further investigation. As a potential guide, PDHK4 can directly phosphorylate SMAD1/5/8 via direct interaction to enhance bone morphogenetic protein 2 signaling and vascular calcification in vascular smooth muscle cells (Lee et al., 2015). PDHK4 was reported to sequester NF-κB/p65 in the cytoplasm via a direct protein-protein interaction in hepatocytes (Wu et al., 2018). These studies together indicate that PDHK4 has a dual location and function. We found that PDHK1 is the most abundant isoform expressed in macrophages. Inhibition of PDHK by DCA or genetic deletion of PDHK1 up-regulated OPA1 expression at both transcript and protein levels, making it likely that PDHK1 may translocate to the cytoplasm to regulate mitochondrial fission/fusion protein expression by phosphorylating transcriptional factors or signaling molecules involved in

this process. Approaches such as phosphoproteomics analysis of subcellular compartments may enlighten PDHK-regulated mitochondrial dynamics independent of PDC.

Autophagy regulates organelle and protein turnover by both degradative and secretory mechanisms. Degradative autophagy inhibits NLRP3 inflammasome activation by inhibiting mitochondrial DNA release (Nakahira et al., 2011), inducing inflammasome complex degradation (Harris et al., 2011; Shi et al., 2012), or clearing damaged mitochondria (Zhou et al., 2011). In contrast, secretory autophagy facilitates the extracellular delivery of IL-1β through an unconventional secretory pathway (Claude-Taupin et al., 2018; Dupont et al., 2011; Iula et al., 2018; Zhang et al., 2015). Therefore, in the autophagy-deficient macrophages, the level of extracellular IL-1β is the net result of the increased IL-1β cleavage due to enhanced inflammasome activation and the attenuated IL-1β secretion due to the impaired unconventional secretory pathway. Nonetheless, our results showed that PDHK inhibition promotes autophagic flux and mitophagy in NLRP3 inflammasome stimulated macrophages. Despite the indispensable role of autophagy in attenuating IL-1β secretion by PDHK inhibition, the enhanced autophagic flux, especially mitophagy, paralleled improved mitochondrial morphology and function in PDHK-inhibited macrophages, suggesting that PDHK inhibition, in part, promotes mitochondrial homeostasis by activating mitophagy.

In conclusion, we discover non-canonical roles for mitochondrial PDHK in supporting mitochondrial oxidative damage and NLRP3 inflammasome activation independent of its canonical regulation of pyruvate oxidation. Although the detailed mechanisms need further elucidation, targeting PDHK dampens NLRP3 inflammasome activity, reverses the metabolic paralysis, and maintains mitochondrial fitness in inflamed macrophages. These aspects promote macrophage homeostasis and health in sepsis, making PDHK inhibition by DCA/JX06 translationally valuable. In addition to sepsis, PDHK has emerged as a critical target in other disease states, including diabetes (Rahman et al., 2020) and cardiovascular diseases (Li et al., 2019). Hence, our study provides evidence for the therapeutic targeting of PDHK to treat inflammatory conditions.

**Limitations of the study**

In this study, we utilized various pharmacological inhibitors to examine the effect of the metabolic pathways on NLRP3 inflammasome activation. Although these inhibitors are well-characterized in the literature, there is still potential that non-specific untargeted effects exist and interfere with the data interpretation. Also, we blocked each targeted pathway using a pathway-specific inhibitor when we examined the impact of metabolic shift induced by PDHK inhibition on the NLRP3 inflammasome. We do not rule out that there could be a combinatory effect through multiple pathways on PDHK-regulated NLRP3 inflammatory activation. Lastly, the metabolic changes in our study were primarily measured by targeted or untargeted metabolomics and Seahorse flux assays. We did not track the carbon flux of specific pathways by stable isotope radiolabeling.

**Acknowledgments**

The authors gratefully acknowledge Ken Grant, Paula Graham, and Debbie Golden of the Cellular Imaging Shared Resource (CISR) of Atrium Health Wake Forest Baptist for technical assistance with confocal and transmission electron microscopy. The authors also would like to acknowledge pilot funding support from the Wake Forest Center for Redox Biology and Medicine (CRBM) and helpful feedback during the CRBM Metabolism and Inflammation working group meetings. This study was supported by NIH R35 GM126922 (CEM), NIH R01 CA248037 (HKL), NIH R01 HL132035 (XZ). AKM was supported by NIH T32GM127261 and NIH T32 AI007401 training grants. The study was also supported by the National Center for Advancing Translational Sciences of the National Institutes of Health under Award Number UL1TR001420 (Research Assistant fund to XZ).

**Author Contributions**

X.Z. conceived the study; A.K.M., Z.W., W.H., Q.Zhao, M.Z., Q.Zhang, and F.L. conducted the experiments; J.L. conducted the high-resolution metabolomics analysis and edited the manuscript; R.K.M provided advice related to TEM; J.W.L. provided advice related to metabolomics analysis, helped with data discussion, and provided comments; M.A.Q, Q.S., D.F., H.K.L., C.M.F., and C.E.M helped with data discussion and provided comments and revisions; Z.W. wrote the methods and edited the manuscript; A.K.M. and X.Z. drafted the manuscript; X.Z. wrote and finalized the manuscript.

**Declaration of Interests**

The authors declare no competing interests.

**Inclusion and diversity statement**

One or more of the authors of this paper self-identified as living with a disability.

## Figure legends

**Figure 1. PDHK inhibition lowers macrophage NLRP3 inflammasome activation and cell death.**

Murine bone marrow-derived macrophages (BMDMs) or human PBMC-derived macrophages were first primed with 300 ng/ml LPS for 3 h, then stimulated with 5mM ATP for 45 min-1 h, 10 μM nigericin (NIG) for 1 h, or 0.6 mg/ml monosodium urate crystals (MSU) for 6 h, respectively.

(**A**) Schematic of macrophage treatments and timing.

(**B-C**) 20 mM DCA, 10 μM JX06, or DMSO (vehicle control for JX06) were added before or after LPS priming. IL IL-1β concentrations in the culture supernatant were analyzed by ELISA.

(**D-E**) 5-20 mM DCA, 5-40 μM JX06, or DMSO (vehicle control for JX06) were added after LPS priming. IL-1β concentrations in the culture supernatant were analyzed by ELISA.

(**F-G**) 5-20 mM DCA, 5-40 μM JX06, or DMSO (vehicle control for JX06) were added after LPS priming. Protein expression in the culture supernatant (Sup) and whole-cell lysates (Lys) was analyzed by immunoblotting.

(**H-I**) 20 mM DCA or 10 μM JX06 were added before or after LPS priming. mRNA expression of NLRP3 inflammasome components was measured by qPCR.

(**J-K**) Cell death was measured by staining macrophages with 7-AAD or PI and analyzed by flow cytometry.

(**L**) 20 mM DCA or 10 μM JX06 were added after LPS priming. Protein expression in the culture supernatant (Sup) and whole-cell lysates (Lys) was analyzed by immunoblotting.

(**M-N**) 20 mM DCA or 10 μM JX06 were added after LPS priming and together with ATP in human macrophages. IL-1β concentrations in the culture supernatant were analyzed by ELISA and protein expression in the culture supernatant (Sup) and whole-cell lysates (Lys) was analyzed by immunoblotting.

Groups with different letters are significantly different ($p<0.05$), one-way ANOVA with post hoc Tukey's multiple comparisons test.

**Figure 2. PDHK inhibition rewires cellular metabolism in NLRP3 inflammasome-activated macrophages.**

Untargeted metabolomics data were collected from LPS (300 ng/ml)-primed BMDMs treated with ATP (5 mM) plus 10 μM JX06 or DMSO as vehicle control for 45 min. The analysis was performed using MetaboAnalyst 5.0.

(**A**) Principal component analysis of the metabolites in BMDMs.

(**B**) Volcano plot of the metabolites in LPS+ATP vs. control macrophages, plotted using Graphpad 7.0.

(**C**) The top 25 enriched metabolic pathways in LPS+ATP treated vs. control BMDMs, identified by enrichment analysis and ranked according to p values.

(**D**) Volcano plot of the metabolites in JX06 vs. LPS+ATP treated macrophages, plotted using Graphpad 7.0

(**E**) The top 10 metabolic pathways altered by JX06 treatment, identified by the pathway analysis and ranked according to p values.

**Figure 3. PDHK inhibition reprograms glycolysis, pentose phosphate pathway (PPP), and TCA cycle metabolism in NLRP3 inflammasome-activated macrophages.**

(**A**) Diagram of glycolysis and PPP.

(**B**) Heatmap of the intermediates in the glycolysis pathway from the untargeted metabolomics analysis.

(**C**) Heatmap of the intermediates in PPP from the untargeted metabolomics analysis.

(**D-E**) Seahorse analysis of extracellular acidification rates (ECAR) in BMDMs treated with LPS (300 ng/ml), LPS (300 ng/ml) + ATP (5 mM) in the presence or absence of DCA (20 mM) or JX06 (10 μM) for 30 min.

(**F**) Glucose uptake in BMDMs treated with LPS (300 ng/ml) + ATP (5 mM) in the presence or absence of DCA (20 mM), JX06 (10 μM), or 2-NBDG (100 μg/ml) for 30 min. Macrophages were analyzed by flow cytometry.

(**G**) Diagram of TCA cycle and its coupling pathways.

(**H**) Heatmap of the intermediates in the TCA cycle.

(**I**) Heatmap of the intermediates in the PC-mediated anaplerosis pathway, aspartate-argininosuccinate shunt, and urea cycle.

(**J-K**) Seahorse analysis of oxygen consumption rates (OCR) in BMDMs treated with LPS (300 ng/ml), LPS (300 ng/ml) + ATP (5 mM) in the presence or absence of DCA (20 mM) or JX06 (10 μM) for 30 min.

(**L-M**) Seahorse XF real-time ATP rate analysis of BMDMs. Glycolytic ATP and mitochondrial ATP production rates were calculated.

Groups with different letters are significantly different ($p<0.05$). $^{\#}$: $p<0.05$, between LPS+ATP and control groups; *: $p<0.05$, between LPS+ATP and LPS+JX06+ATP groups; one-way ANOVA with post hoc Tukey's multiple comparisons test.

**Figure 4. PDHK inhibition-mediated NLRP3 inflammasome inactivation is independent of glucose metabolism or pyruvate dehydrogenase.**

Bone marrow-derived macrophages (BMDMs) or thioglycollate-elicited peritoneal macrophages (PMs) were stimulated with LPS (300 ng/ml) for 3 h and 5 mM ATP for 45 min to induce the NLRP3 inflammasome activation. DCA (20 mM) or JX06 (10 μM) were added after LPS priming.

(**A**) The targeting sites of the pharmacological inhibitors are indicated.

(**B-F**) IL-1β secretion from LPS plus ATP-treated BMDMs. The pharmacological inhibitors were added 30 min before ATP stimulation.

(**G**) Pdhe1a mRNA expression in control and PDHe1α siRNA transfected elicited PMs.

(**H-I**) IL-1β secretion and caspase-1 cleavage in the culture supernatant from control siRNA and Pdhe1α siRNA transfected PMs treated with or without LPS plus ATP in the presence or absence of DCA or JX06.

(**J**) mRNA expression of PDHK isoforms in BMDMs treated with or without LPS plus ATP. Gene expression was normalized to PDHK1 expression in unstimulated macrophages.

(**K**) Transcript expression of PDHK isoform 1 and 2 in control and isoform-specific siRNAs (50 μM) transfected PMs, respectively.

(**L-M**) IL-1β secretion and caspase-1 cleavage in the culture supernatant from control siRNA and isoform-specific siRNA transfected PMs treated with or without LPS plus ATP.

Groups with different letters are significantly different ($p<0.05$); *P < 0.05; **P < 0.01; ***P < 0.001; ****P < 0.0001; ns: non-significant. One-way ANOVA with post hoc Tukey's multiple comparisons test (Figures 5B-5F, 5H, 5L); unpaired, two-tailed student's T-test (Figures 5G, 5J, and 5K).

**Figure 5. Autophagy is unnecessary for down-regulation of the NLRP3 inflammasome by PDHK inhibition.**

(**A**) Bone marrow-derived macrophages (BMDMs) were primed with 300 ng/ml LPS for 3 h, followed by 5 mM ATP in the presence or absence of 20 mM DCA or 10 μM JX06 for 0-120 min. Immunoblotting analysis of LC3 expression in BMDMs. 50 nM bafilomycin A1 was added together with ATP to monitor the autophagic flux.

(**B**) Immunoblotting analysis of mitophagy marker expression in BMDMs as described in (**A**) except for bafilomycin A1 treatment.

(**C**) Atg5 mRNA expression in macrophages.

(**D-E**) IL-1β secretion and caspase-1 cleavage in the culture supernatant from WT and Atg5$^{-/-}$ BMDMs treated with or without LPS (300 ng/ml) plus ATP (5 mM) in the presence or absence of DCA (20 mM) or JX06 (10 μM) for 45 min.

**(F)** BMDMs were pre-incubated with 3-methyladenine (3-MA, 5 mM) for 30 min before treated with or without LPS (300 ng/ml) plus ATP (5 mM) in the presence or absence of DCA (20 mM) or JX06 (10 μM) for 45 min. IL-1β concentration in the culture supernatant was measured by ELISA.

*P < 0.05; ****P < 0.0001; ns: non-significant. Unpaired, two-tailed student's T-test (Figure 5C). Two-way ANOVA with post hoc Tukey's multiple comparisons test (Figures 5D and 5F).

**Figure 6. PDHK inhibition-mediated NLRP3 inflammasome inactivation is independent of mitochondrial OPA1 or ROS production.**

Bone marrow-derived macrophages (BMDMs) or thioglycollate elicited peritoneal macrophages (PMs) were primed with 300 ng/ml LPS for 3 h, followed by 5 mM ATP in the presence or absence of 20 mM DCA or 10 μM JX06 for 45 min unless indicated here.

(**A**) BMDMs were stained with MitoSOX (5 μM) and mitochondrial ROS was analyzed by flow cytometry.

(**B**) Confocal images of BMDMs stained with MitoTracker Deep Red (red) and DAPI (blue). Scale bar=5 nm.

(**C**) Representative transmission electron microscopy (TEM) images of BMDMs. Scale bar=500 nm.

(**D-E**) Mitochondrial length and perimeter were quantified.

(**F**) Representative mitochondrial TEM images. Scale bar=100 nm.

(**G-H**) Mitochondrial cristae number per mitochondrion and cristae width.

(**I**) Immunoblotting analysis of p-Drp1 (ser616) and OPA1 in LPS primed BMDMs, followed by ATP plus DCA treatment for 0-120 min.

(**J**) Opa1 transcript expression in PDHK1-silenced PMs.

(**K**) Immunoblotting analysis of OPA1 and p-Drp1 (ser616) in PMs. Macrophages were first transfected with control siRNA and 50 μM PDHK1 siRNAs before treated with or without LPS plus ATP.

(**L**) Immunoblotting analysis of OPA1 protein expression in PMs treated with control and OPA1 siRNAs at 25 to 100 μM for 72 h.

(**M**) IL-1β level in the culture supernatant from OPA1 silenced PMs treated with or without LPS plus ATP in the presence or absence of DCA. PMs were treated with 100 μM control and OPA1 siRNAs for 72 h before LPS and ATP stimulation.

(**N-O**) 10 or 50 μM mitoParaquat (MitoPQ) were added to PS primed macrophages 30 min before ATP stimulation in the presence or absence of DCA. BMDMs were stained with MitoSOX (5 μM) and mitochondrial ROS was analyzed by flow cytometry (N). Culture supernatant was analyzed for IL-1β by ELISA (O).

***, P<0.001. Groups with different letters are significantly different (p<0.05) Unpaired, two-tailed student's T-test (Figure JC). One-way ANOVA with post hoc Tukey's multiple comparisons test (Figures 6A, 6D, 6E, 6G, 6H, 6N, and 6O). Two-way ANOVA with post hoc Tukey's multiple comparisons test (Figure 6M).

**Figure 7. PDHK inhibition lowers plasma IL-1β and blood monocyte and neutrophil caspase-1 activity in septic mice.**

Mice were i.p. injected with 25 mg/kg DCA or saline as vehicle control 24 h post cecal ligation and puncture. Sham-operated mice were used as another control. Blood was collected 6 h after DCA injection.

(**A**) Schematic of mouse treatments.

(**B-D**) Plasma IL-1β, IL-18, and lactate dehydrogenase (LDH) were measured by ELISA.

(**E-G**) Percentage of blood monocytes ($CD115^{+}Ly6G^{-}$) and neutrophils ($CD115^{-}Ly6G^{+}$) in $CD45^{+}$ cells were analyzed by flow cytometry.

(**H-I**) The percentage of FAM-YVAD-FMK probe $(FLICA)^{+}$ cells in blood monocytes ($CD45^{+}CD115^{+}Ly6G^{-}$) was analyzed by flow cytometry.

(**J-K**) The percentage of $FLICA^{+}$ cells in blood neutrophils ($CD45^{+}CD115^{-}Ly6G^{+}$) was analyzed by flow cytometry.

Each symbol represents an individual mouse. *P < 0.05; **P < 0.01; ***P < 0.001; ns: non-significant, one-way ANOVA with post hoc Tukey's multiple comparisons test.

## Star Methods

### Resource availability

### Lead contract

Further information and request for resources and reagents should be directed to and will be fulfilled by the lead contact, Xuewei Zhu (xwzhu@wakehealth.edu)

### Materials availability

All unique reagents generated in this study are available from the lead contact without restriction.

### Data Availability

Untargeted metabolomics data were deposited in MetaboLights (Haug et al., 2020) under Study MTBL3632, https://www.ebi.ac.uk/metabolights/MTBLS3632 (Control; LA=LPS+ATP; LJA= LPS+JX06+ATP).

### Methods details

### Mice

C57BL/6J (stock 000664), LysMcre (stock 004781), and Gsdmd$^{-/-}$ (stock 032410) mice were purchased from Jackson Laboratories. Atg5$^{flox/flox}$ mice were purchased from Riken BioResource Center (stock RBRC02975). Heterozygous atg5 macrophage-specific knockout (atg5$^{flox/+}$Lyscre$^{+}$) mice were generated by crossing atg5$^{flox/flox}$ mice and LysMcre mice. Homozygous atg5 macrophage-specific knockout (atg5$^{flox/flox}$LysMcre$^{+}$) and WT control mice (atg5$^{flox/flox}$) were generated by intercrossing the heterozygous mice, as described previously (Shen et al., 2017). Mice were housed in a pathogen-free facility on a 12 h light/dark cycle and received a standard laboratory diet. Cecal ligation and puncture (CLP) were performed to induce intra-abdominal polymicrobial infection in C57 BL/6J male mice at the age of 12 weeks as described previously (McCall et al., 2018). Sham-operated mice were used as a control. DCA (25 mg/kg) or saline was injected intraperitoneally (i.p.) 24 h post-CLP. Mice were euthanized 30 hours post CLP. All animal experimental protocols were approved by the Wake Forest University Animal Care and Use Committee.

### Cell culture and treatment

Bone marrow-derived macrophages (BMDM) and thioglycollate-elicited peritoneal macrophages were cultured as described previously (Wang et al., 2020; Zhu et al., 2008). Briefly, mouse bone marrow was cultured in low glucose DMEM supplemented with 30% L929 cell-conditioned medium, 20% FBS, 2 mM L-glutamine, 1 mM sodium pyruvate, 100 U/ml penicillin, and 100 µg/ml streptomycin for 6-7 days until the cells reached confluence. BMDMs were then reseeded in culture dishes overnight in RPMI-1640 medium containing 1% Nutridoma-SP medium (Sigma-Aldrich) before any treatment. Thioglycollate-elicited peritoneal macrophages (PMs) were harvested from mice by washing peritoneal cavities using cold PBS 3 days after i.p. injection of 1 ml of 10% thioglycollate (Sigma-Aldrich). After a 2 h Incubation in RPMI-1640 media containing 10% FBS, 100 U/ml penicillin, and 100 µg/ml streptomycin, floating cells were removed, and adherent macrophages were used for experiments. Peripheral blood mononuclear cells (PBMCs) were isolated from fresh blood from a healthy donor using 1:1 ratio of blood to Histopaque 1077. PBMCs were subsequently cultured in RPMI-1640

medium supplemented with M-CSF (100 ng/mL), 20% FBS, 2 mM L-glutamine, 1 mM sodium pyruvate, 100 U/ml penicillin, and 100 μg/ml streptomycin for 6-7 days until the cells reach confluence. PBMCs-derived macrophages were replaced in culture dishes before inflammatory stimulation. The study protocol was approved by the Wake Forest University Institutional Review Board.

To induce NLRP3 inflammasome activation, macrophages were first primed with 300 ng/ml LPS (E. coli 0111; B4, Sigma-Aldrich) before stimulated with 5 mM ATP (Sigma-Aldrich) for 15 min to 120 min, 10 μM nigericin (InvivoGen) for 1 h, 0.6 mg/ml monosodium urate crystals (MSU) (InvivoGen) for 6 h in RPMI-160 medium, as indicated in the figure legends. To assess the AIM2 inflammasome, BMDMs were first primed with 300 ng/ml LPS for 3h before stimulated with poly dA:dT (2.5 μg/mL, InvivioGen) complexed with transfection reagent LyoVec for 7 hours. To inhibit PDHK, macrophages were pretreated for 30 min before LPS priming or after LPS priming (together with inflammasome stimuli as described above) with DCA (5-30 mM, Sigma-Aldrich), JX06 (5-40 μM, Rocris) for an indicated time as described in the figure legends. In some experiments, LPS-primed macrophages were treated with AOAA (1 mM, Cayman Chemical), bafilomycin A1 (50 nM, In vivoGen), chlorothricin (100 μM, Cayman Chemical), CPI-613 (200 μM, Cayman Chemical), 2-DG (10 mM, Sigma-Aldrich), DHEA (200 μM, Sigma-Aldrich), dorsomorphin (10 μM, MedChemExpress), etomoxir (50 μM, Cayman Chemical), fumonisin B1 (15 μM, Cayman Chemical), glycine (5 mM, Sigma-Aldrich), heptelidic acid (15 μM, Cayman Chemical), 3-MA (5 mM, Sigma-Aldrich), ML385 (5 μM, MedChemExpress), SC-26196 (10 μM, Cayman Chemical), sodium oxamate (40 mM, Santa Cruz Biotechnology), U0126 (25 μM, Calbiochem), or UK5099 (5 μM, Cayman Chemical), as indicated in the figure legends. PBS, DMSO, or ethanol was used as vehicle control in the inhibitor experiments.

**Flow cytometry**

After removing the red blood cells using ACK lysing buffer (Gibco), peripheral white blood cells were stained with FLICA 660-YVAD-FMK (1:150 dilution, ImmunoChemistry Technologies), CD115-PE (eBioscience, no. 12-1152), Gr1(Ly6C/G)-PerCP-Cy5.5 (BioLegend, no. 108427), and CD45-APC (BD Pharmingen, no. 559864). Data were acquired on a BD FACS Canto II instrument (BD Biosciences) and analyzed using FlowJo analytical software (version 7.6.5, TreeStar). To measure cell death, BMDMs were stained with 7-AAD (Invitrogen, cat# V35123) or PI (Invitrogen, Cat# P3566) according to the manufacturer's instructions. To quantify glucose uptake, BMDMs were exposed to 100 μg/ml 2-NBDG (Cayman Chemical, Cas#186689-07-6) after LPS priming for 30 min. Data were acquired on a BD FACSCalibur and analyzed using FlowJo analytical software (version 7.6.5, TreeStar).

**High-resolution untargeted metabolomics**

LPS-primed BMDMs were stimulated with 5 mM ATP in the presence or absence of 10 μM JX06 for 45 min. Unstimulated macrophages were used as control. Macrophages were lysed, and polar metabolites were

extracted using methanol and $H_2O$ (80:20; HPLC Grade; Sigma-Aldrich) (Liu et al., 2015). Extracts were dried under nitrogen gas, followed by liquid chromatography using Ultimate 3000 UHPLC (Dionex) coupled to high-resolution-mass spectrometry for metabolite profiling using the Q Exactive Plus-Mass spectrometer (QE-MS, Thermo Scientific) (Liu et al., 2014). Commercial software Sieve 2.2 (Thermo Scientific) was using for peak extraction and integration. Liquid chromatography-mass spectrometry peak areas were normalized to sample protein mass measured by the BCA assay. Pathway analysis of metabolites was conducted using the MetaboAnalyst v.5.0.

**Targeted metabolomics**

LPS-primed BMDMs were stimulated with 5 mM ATP in the presence or absence of 10 μM JX06 for 30 min. Unstimulated macrophages were used as control. Macrophages were lysed, and polar metabolites were extracted using methanol and $H_2O$ (80:20; HPLC Grade; Sigma-Aldrich) (Liu et al., 2015). 500 μl of cell extracts and 20 μl of MES (Thermo Fisher Scientific) internal standard solution (10 ng/μl) were mixed and dried under vacuum and reconstituted for analysis in 100 μl of ultrapure water (Optima, ThermoFisher Scientific). The analysis was performed on a Shimadzu Nexera UHPLC system coupled with a Shimadzu LCMS-8050 triple-quadrupole mass spectrometer (Kyoto, Japan). Two LC-MS/MS methods (Ion-paring and PFPP) were employed to measure the targets. Data were normalized to sample protein mass measured by the BCA assay.

**Microscopy analysis**

*DIC imaging*

DIC images of BMDMs were obtained using a Zeiss Axio Vert.A1 microscope with AxioCam ICc3 camera. Cells in more than 5 fields of a 20x objective were analyzed for cell size using NIH ImageJ software (NIH).

*Confocal imaging*

BMDMs seeded in a glass chamber slide were stained with 100 nM MitoTracker Deep Red (Invitrogen) for 15 min at 37 $^{o}$C in dark. Macrophages were then washed and fixed with 4% paraformaldehyde. Nuclei were stained using DAPI. Confocal images were obtained with a FV1200 laser-scanning confocal microscope (Olympus).

*Transmission electron microscopy (TEM) imaging*

BMDMs were subjected to TEM imaging in the Wake Forest Baptist Health Electron Microscope Core Lab. Briefly, macrophages were fixed in 2.5% glutaraldehyde in 0.1 M Millonig's phosphate buffer pH 7.3 for a minimum of 1 h, wash with buffer, and post-fixed in % osmium tetroxide for 1 h. After dehydration, resin infiltration, and cure in a 70 $^{o}$C oven overnight, cells were sectioned on a Reichert-Jung Ultracut E ultramicrotome. The sections were then stained with lead citrate and uranyl acetate and viewed with an FEI. Tecnai Spirit TEM was operating at 80 kV. Images were obtained with an AMT 2Vu CCD Camera.

Mitochondrial morphology was analyzed on images with 4800x or 18500x magnification. More than 20 cells or 70 to 100 mitochondria per group were analyzed to quantify mitochondrial or cristae ultrastructure changes using NIH ImageJ software (NIH).

**Mitochondrial ROS (mtROS) measurement**

mtROS production in BMDMs was measured by MitoSOX (Fisher Scientific, no. M36008) staining (5 µM for 15 min at 37°C). Macrophages were washed with PBS and scraped off the dishes. Data were acquired on a BD FACSCalibur and analyzed using FlowJo analytical software (version 7.6.5, TreeStar).

**Seahorse assays**

2 x $10^5$ BMDMs were plated into each well of Seahorse XF96 cell culture microplates (Agilent Technologies) and cultured overnight in in 1% Nutridoma SP medium before treated with or without LPS for 3 h plus ATP for 30 min. Cells were washed with designed seahorse media and continued to be incubated in the seahorse media for another 30 min. Extracellular acidification rate (ECAR), oxygen consumption rate (OCR), and real-time ATP production rate in BMDMs were measured by using glycolysis stress kit, mitochondrial stress kit, and real-time ATP rate assay kit, respectively, with a Seahorse XF96 Extracellular Flux Analyzer (Agilent Technologies). 10 mM glucose, 1 µM oligomycin, 1.5 µM fluoro-carbonyl cyanide phenylhydrazone (FCCP), 100 nM rotenone plus 1 µM antimycin A, or 50 mM 2DG (all the compounds were from Agilent Technologies) were sequentially injected into the microplates according to the manufacturer's instructions. After the assay, 3 µM Hoechst (Life Technologies) was added to each well to stain nuclei for cell counting. Results were collected with Wave software version 2.6 (Agilent Technologies). Data were normalized to cell numbers.

**siRNA transfection**

25-100 nM control, PDHK1, PDHK2, PDHK4, PDHE1a, or OPA1 ON-Targetplus siRNAs (Dharmacon, Lafayette, CO) were transfected into elicited peritoneal macrophages isolated from WT C57BL/6 mice with DharmaFECT 1 transfection reagent (Dharmacon, Lafayette, CO) according to the manufacturer's protocol. siRNA transfection efficiency was quantified by qPCR or western blotting.

**ELISA**

Mouse IL-1β, IL-18, TNF, IL-6, or LDH were measured in macrophage culture supernatants or mouse plasma using commercially available ELISA kits according to the manufacturer's instructions.

**qPCR**

Total RNA was isolated from macrophages using Trizol reagent (Thermo Fisher Scientific). cDNA was synthesized with Omniscript RT Kit (Qiagen). The relative mRNA expression level of each target gene was

quantified by qPCR using KAPA SYBR fast qPCR master mix (Roche). Data were normalized to GAPDH and expressed relative to control unstimulated macrophages. The sequences of the primers are listed in Table S1.

**Western Blotting**

Macrophage cell lysates were lysed in radioimmunoprecipitation assay (RIPA) buffer containing protease inhibitor cocktails and PhosSTOP (Roche). Protein concentration was measured using the BCA Protein Assay Kit (Pierce). Primary antibodies used were anti-caspase-1 p20 (AdipoGen, no. AG-20B-0042; 1:1000), LC-3 (Novus Biologicals, no. NB100-2220; 1:500), P62 (Novus Biologicals, no. NBP1-48320; 1:4000), NLRP3 (Adipogen, no. AG-20B-0014; 1:1000), ASC (Adipogen, no. AG-25B-0006; 1:1000), PDHe1α (ThermoFisher, no. PA5-21536; 1:1000), p-AMPK (Cell Signaling, no. 50081s; 1:1000), TUFM (Novus Biologicals, no. CL2242; 1:500), GAPDH (Invitrogen, no. MA5-15738; 1:10,000), OPA1 (Cell Signaling, no. CST80471; 1:1000), p-DRP1 (Ser616) (Cell Signaling, no. 3455S; 1:500), p-TBK1 (Ser172) (Cell Signaling, no. CST5483; 1:1000), p-Erk1/2 (Cell Signaling, no. 9101; 1:1000), Erk1/2 (Cell Signaling, no. 9102; 1:1000), and β-actin (Sigma-Aldrich, no. A5441; 1:5000). Immunoblots were visualized with the Supersignal substrate system (Thermo Fisher Scientific), and chemiluminescence was captured using the ChemiDox MP imaging system (Bio-Rad) or an LSA-3000 imaging system (Fujifilm Life Science).

**Statistics**

In vitro experiments were performed in triplicate or quadruplicate except for the seahorse assays which were performed in at least quadruplicate. Individual dots in each graph represented individual data points for *in vivo* and *in vitro* experiments. At least two independent experiments were performed for each assay except for the metabolomics analysis. Statistical analysis was performed using GraphPad Prism software 7 (GraphPad Software). Data are presented as the mean ± SEM unless indicated otherwise. Differences were compared with Student's t-test, one-way ANOVA or two-way ANOVA with post hoc Tukey's multiple comparison test. Significant differences were regarded as $p < 0.05$, $p < 0.01$, $p < 0.001$, or $p < 0.0001$, indicated in the figure legends.

**Graphical Representations**

Schematics and graphical abstract were created using BioRender online software.

**References**

Aachoui, Y., Leaf, I.A., Hagar, J.A., Fontana, M.F., Campos, C.G., Zak, D.E., Tan, M.H., Cotter, P.A., Vance, R.E., Aderem, A.*, et al.* (2013). Caspase-11 protects against bacteria that escape the vacuole. Science (New York, NY) *339*, 975-978.

Bambouskova, M., Potuckova, L., Paulenda, T., Kerndl, M., Mogilenko, D.A., Lizotte, K., Swain, A., Hayes, S., Sheldon, R.D., Kim, H.*, et al.* (2021). Itaconate confers tolerance to late NLRP3 inflammasome activation. Cell reports *34*, 108756.

Billingham, L.K., Stoolman, J.S., Vasan, K., Rodriguez, A.E., Poor, T.A., Szibor, M., Jacobs, H.T., Reczek, C.R., Rashidi, A., Zhang, P.*, et al.* (2022). Mitochondrial electron transport chain is necessary for NLRP3 inflammasome activation. Nature immunology *23*, 692-704.

Broz, P., Newton, K., Lamkanfi, M., Mariathasan, S., Dixit, V.M., and Monack, D.M. (2010). Redundant roles for inflammasome receptors NLRP3 and NLRC4 in host defense against Salmonella. The Journal of experimental medicine *207*, 1745-1755.

Broz, P., Ruby, T., Belhocine, K., Bouley, D.M., Kayagaki, N., Dixit, V.M., and Monack, D.M. (2012). Caspase-11 increases susceptibility to Salmonella infection in the absence of caspase-1. Nature *490*, 288-291.

Cereghetti, G.M., Stangherlin, A., Martins de Brito, O., Chang, C.R., Blackstone, C., Bernardi, P., and Scorrano, L. (2008). Dephosphorylation by calcineurin regulates translocation of Drp1 to mitochondria. Proceedings of the National Academy of Sciences of the United States of America *105*, 15803-15808.

Chen, X., He, W.T., Hu, L., Li, J., Fang, Y., Wang, X., Xu, X., Wang, Z., Huang, K., and Han, J. (2016). Pyroptosis is driven by non-selective gasdermin-D pore and its morphology is different from MLKL channel-mediated necroptosis. Cell research *26*, 1007-1020.

Cheng, S.C., Scicluna, B.P., Arts, R.J., Gresnigt, M.S., Lachmandas, E., Giamarellos-Bourboulis, E.J., Kox, M., Manjeri, G.R., Wagenaars, J.A., Cremer, O.L.*, et al.* (2016). Broad defects in the energy metabolism of leukocytes underlie immunoparalysis in sepsis. Nature immunology *17*, 406-413.

Claude-Taupin, A., Bissa, B., Jia, J., Gu, Y., and Deretic, V. (2018). Role of autophagy in IL-1β export and release from cells. Seminars in cell & developmental biology *83*, 36-41.

Cogliati, S., Frezza, C., Soriano, M.E., Varanita, T., Quintana-Cabrera, R., Corrado, M., Cipolat, S., Costa, V., Casarin, A., Gomes, L.C.*, et al.* (2013). Mitochondrial cristae shape determines respiratory chain supercomplexes assembly and respiratory efficiency. Cell *155*, 160-171.

Cruz, C.M., Rinna, A., Forman, H.J., Ventura, A.L., Persechini, P.M., and Ojcius, D.M. (2007). ATP activates a reactive oxygen species-dependent oxidative stress response and secretion of proinflammatory cytokines in macrophages. The Journal of biological chemistry *282*, 2871-2879.

Danielski, L.G., Giustina, A.D., Bonfante, S., Barichello, T., and Petronilho, F. (2020). The NLRP3 Inflammasome and Its Role in Sepsis Development. Inflammation *43*, 24-31.

Deretic, V. (2021). Autophagy in inflammation, infection, and immunometabolism. Immunity *54*, 437-453.

Dupont, N., Jiang, S., Pilli, M., Ornatowski, W., Bhattacharya, D., and Deretic, V. (2011). Autophagy-based unconventional secretory pathway for extracellular delivery of IL-1β. The EMBO journal *30*, 4701-4711.
Fang, R., Tsuchiya, K., Kawamura, I., Shen, Y., Hara, H., Sakai, S., Yamamoto, T., Fernandes-Alnemri, T., Yang, R., Hernandez-Cuellar, E.*, et al.* (2011). Critical roles of ASC inflammasomes in caspase-1 activation and host innate resistance to Streptococcus pneumoniae infection. Journal of immunology (Baltimore, Md : 1950) *187*, 4890-4899.
Ferreira, A.C., Soares, V.C., de Azevedo-Quintanilha, I.G., Dias, S., Fintelman-Rodrigues, N., Sacramento, C.Q., Mattos, M., de Freitas, C.S., Temerozo, J.R., Teixeira, L.*, et al.* (2021). SARS-CoV-2 engages inflammasome and pyroptosis in human primary monocytes. Cell death discovery *7*, 43.
Geisler, S., Holmström, K.M., Skujat, D., Fiesel, F.C., Rothfuss, O.C., Kahle, P.J., and Springer, W. (2010). PINK1/Parkin-mediated mitophagy is dependent on VDAC1 and p62/SQSTM1. Nature cell biology *12*, 119-131.
Hagar, J.A., Powell, D.A., Aachoui, Y., Ernst, R.K., and Miao, E.A. (2013). Cytoplasmic LPS activates caspase-11: implications in TLR4-independent endotoxic shock. Science (New York, NY) *341*, 1250-1253.
Harris, J., Hartman, M., Roche, C., Zeng, S.G., O'Shea, A., Sharp, F.A., Lambe, E.M., Creagh, E.M., Golenbock, D.T., Tschopp, J.*, et al.* (2011). Autophagy controls IL-1beta secretion by targeting pro-IL-1beta for degradation. The Journal of biological chemistry *286*, 9587-9597.
Haug, K., Cochrane, K., Nainala, V.C., Williams, M., Chang, J., Jayaseelan, K.V., and O'Donovan, C. (2020). MetaboLights: a resource evolving in response to the needs of its scientific community. Nucleic acids research *48*, D440-d444.
Hooftman, A., Angiari, S., Hester, S., Corcoran, S.E., Runtsch, M.C., Ling, C., Ruzek, M.C., Slivka, P.F., McGettrick, A.F., Banahan, K.*, et al.* (2020). The Immunomodulatory Metabolite Itaconate Modifies NLRP3 and Inhibits Inflammasome Activation. Cell metabolism *32*, 468-478.
Humphries, F., Shmuel-Galia, L., Ketelut-Carneiro, N., Li, S., Wang, B., Nemmara, V.V., Wilson, R., Jiang, Z., Khalighinejad, F., Muneeruddin, K.*, et al.* (2020). Succination inactivates gasdermin D and blocks pyroptosis. Science (New York, NY) *369*, 1633-1637.
Ichinohe, T., Yamazaki, T., Koshiba, T., and Yanagi, Y. (2013). Mitochondrial protein mitofusin 2 is required for NLRP3 inflammasome activation after RNA virus infection. Proceedings of the National Academy of Sciences of the United States of America *110*, 17963-17968.
Iula, L., Keitelman, I.A., Sabbione, F., Fuentes, F., Guzman, M., Galletti, J.G., Gerber, P.P., Ostrowski, M., Geffner, J.R., Jancic, C.C.*, et al.* (2018). Autophagy Mediates Interleukin-1β Secretion in Human Neutrophils. Frontiers in immunology *9*, 269.
Iyer, S.S., He, Q., Janczy, J.R., Elliott, E.I., Zhong, Z., Olivier, A.K., Sadler, J.J., Knepper-Adrian, V., Han, R., Qiao, L.*, et al.* (2013). Mitochondrial cardiolipin is required for Nlrp3 inflammasome activation. Immunity *39*, 311-323.

Junqueira, C., Crespo, Â., Ranjbar, S., de Lacerda, L.B., Lewandrowski, M., Ingber, J., Parry, B., Ravid, S., Clark, S., Schrimpf, M.R.*, et al.* (2022). FcγR-mediated SARS-CoV-2 infection of monocytes activates inflammation. Nature *606*, 576-584..

Karpova, T., Danchuk, S., Kolobova, E., and Popov, K.M. (2003). Characterization of the isozymes of pyruvate dehydrogenase phosphatase: implications for the regulation of pyruvate dehydrogenase activity. Biochimica et biophysica acta *1652*, 126-135.

Kayagaki, N., Stowe, I.B., Lee, B.L., O'Rourke, K., Anderson, K., Warming, S., Cuellar, T., Haley, B., Roose-Girma, M., Phung, Q.T.*, et al.* (2015). Caspase-11 cleaves gasdermin D for non-canonical inflammasome signalling. Nature *526*, 666-671.

Kayagaki, N., Warming, S., Lamkanfi, M., Vande Walle, L., Louie, S., Dong, J., Newton, K., Qu, Y., Liu, J., Heldens, S.*, et al.* (2011). Non-canonical inflammasome activation targets caspase-11. Nature *479*, 117-121.

Kayagaki, N., Wong, M.T., Stowe, I.B., Ramani, S.R., Gonzalez, L.C., Akashi-Takamura, S., Miyake, K., Zhang, J., Lee, W.P., Muszynski, A.*, et al.* (2013). Noncanonical inflammasome activation by intracellular LPS independent of TLR4. Science (New York, NY) *341*, 1246-1249.

Kim, M.J., Yoon, J.H., and Ryu, J.H. (2016). Mitophagy: a balance regulator of NLRP3 inflammasome activation. BMB reports *49*, 529-535.

Klyuyeva, A., Tuganova, A., Kedishvili, N., and Popov, K.M. (2019). Tissue-specific kinase expression and activity regulate flux through the pyruvate dehydrogenase complex. The Journal of biological chemistry *294*, 838-851.

Lee, S.J., Jeong, J.Y., Oh, C.J., Park, S., Kim, J.Y., Kim, H.J., Doo Kim, N., Choi, Y.K., Do, J.Y., Go, Y.*, et al.* (2015). Pyruvate Dehydrogenase Kinase 4 Promotes Vascular Calcification via SMAD1/5/8 Phosphorylation. Scientific reports *5*, 16577.

Lei, Y., Wen, H., Yu, Y., Taxman, D.J., Zhang, L., Widman, D.G., Swanson, K.V., Wen, K.W., Damania, B., Moore, C.B.*, et al.* (2012). The mitochondrial proteins NLRX1 and TUFM form a complex that regulates type I interferon and autophagy. Immunity *36*, 933-946.

Li, X., Liu, J., Hu, H., Lu, S., Lu, Q., Quan, N., Rousselle, T., Patel, M.S., and Li, J. (2019). Dichloroacetate Ameliorates Cardiac Dysfunction Caused by Ischemic Insults Through AMPK Signal Pathway-Not Only Shifts Metabolism. Toxicological sciences : an official journal of the Society of Toxicology *167*, 604-617.

Lin, J., Chen, K., Chen, W., Yao, Y., Ni, S., Ye, M., Zhuang, G., Hu, M., Gao, J., Gao, C.*, et al.* (2020). Paradoxical Mitophagy Regulation by PINK1 and TUFm. Molecular cell *80*, 607-620.e612.

Liu, T.F., Vachharajani, V.T., Yoza, B.K., and McCall, C.E. (2012). NAD+-dependent sirtuin 1 and 6 proteins coordinate a switch from glucose to fatty acid oxidation during the acute inflammatory response. The Journal of biological chemistry *287*, 25758-25769.

Liu, X., Sadhukhan, S., Sun, S., Wagner, G.R., Hirschey, M.D., Qi, L., Lin, H., and Locasale, J.W. (2015). High-Resolution Metabolomics with Acyl-CoA Profiling Reveals Widespread Remodeling in Response to Diet. Molecular & cellular proteomics: MCP *14*, 1489-1500.

Liu, X., Ser, Z., and Locasale, J.W. (2014). Development and quantitative evaluation of a high-resolution metabolomics technology. Analytical chemistry *86*, 2175-2184.
Mainali, R., Zabalawi, M., Long, D., Buechler, N., Quillen, E., Key, C.C., Zhu, X., Parks, J.S., Furdui, C., Stacpoole, P.W.*, et al.* (2021). Dichloroacetate reverses sepsis-induced hepatic metabolic dysfunction. eLife *10,* e64611.
McCall, C.E., Zabalawi, M., Liu, T., Martin, A., Long, D.L., Buechler, N.L., Arts, R.J.W., Netea, M., Yoza, B.K., Stacpoole, P.W.*, et al.* (2018). Pyruvate dehydrogenase complex stimulation promotes immunometabolic homeostasis and sepsis survival. JCI insight *3,* e99292.
Meiser, J., Krämer, L., Sapcariu, S.C., Battello, N., Ghelfi, J., D'Herouel, A.F., Skupin, A., and Hiller, K. (2016). Pro-inflammatory Macrophages Sustain Pyruvate Oxidation through Pyruvate Dehydrogenase for the Synthesis of Itaconate and to Enable Cytokine Expression. The Journal of biological chemistry *291*, 3932-3946.
Meyers, A.K., and Zhu, X. (2020). The NLRP3 Inflammasome: Metabolic Regulation and Contribution to Inflammaging. Cells *9, 1808*.
Mills, E.L., Kelly, B., Logan, A., Costa, A.S., Varma, M., Bryant, C.E., Tourlomousis, P., Dabritz, J.H., Gottlieb, E., Latorre, I.*, et al.* (2016). Succinate Dehydrogenase Supports Metabolic Repurposing of Mitochondria to Drive Inflammatory Macrophages. Cell *167*, 457-470.e413.
Misawa, T., Saitoh, T., Kozaki, T., Park, S., Takahama, M., and Akira, S. (2015). Resveratrol inhibits the acetylated alpha-tubulin-mediated assembly of the NLRP3-inflammasome. International immunology *27*, 425-434.
Misawa, T., Takahama, M., Kozaki, T., Lee, H., Zou, J., Saitoh, T., and Akira, S. (2013). Microtubule-driven spatial arrangement of mitochondria promotes activation of the NLRP3 inflammasome. Nature immunology *14*, 454-460.
Mishra, P., Carelli, V., Manfredi, G., and Chan, D.C. (2014). Proteolytic cleavage of Opa1 stimulates mitochondrial inner membrane fusion and couples fusion to oxidative phosphorylation. Cell metabolism *19*, 630-641.
Moon, J.S., Lee, S., Park, M.A., Siempos, II, Haslip, M., Lee, P.J., Yun, M., Kim, C.K., Howrylak, J., Ryter, S.W.*, et al.* (2015). UCP2-induced fatty acid synthase promotes NLRP3 inflammasome activation during sepsis. The Journal of clinical investigation *125*, 665-680.
Nakahira, K., Haspel, J.A., Rathinam, V.A., Lee, S.J., Dolinay, T., Lam, H.C., Englert, J.A., Rabinovitch, M., Cernadas, M., Kim, H.P.*, et al.* (2011). Autophagy proteins regulate innate immune responses by inhibiting the release of mitochondrial DNA mediated by the NALP3 inflammasome. Nature immunology *12*, 222-230.
Oh, T.S., Zabalawi, M., Jain, S., Long, D., Stacpoole, P.W., McCall, C.E., and Quinn, M.A. (2022). Dichloroacetate improves systemic energy balance and feeding behavior during sepsis. JCI insight *7*. e153944.
Pan, P., Shen, M., Yu, Z., Ge, W., Chen, K., Tian, M., Xiao, F., Wang, Z., Wang, J., Jia, Y.*, et al.* (2021). SARS-CoV-2 N protein promotes NLRP3 inflammasome activation to induce hyperinflammation. Nature communications *12*, 4664.

Park, S., Won, J.H., Hwang, I., Hong, S., Lee, H.K., and Yu, J.W. (2015). Defective mitochondrial fission augments NLRP3 inflammasome activation. Scientific reports *5*, 15489.

Patel, M.S., Nemeria, N.S., Furey, W., and Jordan, F. (2014). The pyruvate dehydrogenase complexes: structure-based function and regulation. The Journal of biological chemistry *289*, 16615-16623.

Pereira, A.C., Madeira, N., Morais, S., Macedo, A., Cruz, M.T., and Pereira, C.M.F. (2022). Mitochondria Fusion upon SERCA Inhibition Prevents Activation of the NLRP3 Inflammasome in Human Monocytes. Cells *11,* 433.

Prieto, J., León, M., Ponsoda, X., Sendra, R., Bort, R., Ferrer-Lorente, R., Raya, A., López-García, C., and Torres, J. (2016). Early ERK1/2 activation promotes DRP1-dependent mitochondrial fission necessary for cell reprogramming. Nature communications *7*, 11124.

Rahman, M.H., Bhusal, A., Kim, J.H., Jha, M.K., Song, G.J., Go, Y., Jang, I.S., Lee, I.K., and Suk, K. (2020). Astrocytic pyruvate dehydrogenase kinase-2 is involved in hypothalamic inflammation in mouse models of diabetes. Nature communications *11*, 5906.

Rathinam, V.A., Vanaja, S.K., Waggoner, L., Sokolovska, A., Becker, C., Stuart, L.M., Leong, J.M., and Fitzgerald, K.A. (2012). TRIF licenses caspase-11-dependent NLRP3 inflammasome activation by gram-negative bacteria. Cell *150*, 606-619.

Sefik, E., Qu, R., Junqueira, C., Kaffe, E., Mirza, H., Zhao, J., Brewer, J.R., Han, A., Steach, H.R., Israelow, B.*, et al.* (2022). Inflammasome activation in infected macrophages drives COVID-19 pathology. Nature *606*, 585-593.

Shen, L., Yang, Y., Ou, T., Key, C.C., Tong, S.H., Sequeira, R.C., Nelson, J.M., Nie, Y., Wang, Z., Boudyguina, E.*, et al.* (2017). Dietary PUFAs attenuate NLRP3 inflammasome activation via enhancing macrophage autophagy. Journal of lipid research *58*, 1808-1821.

Shi, C.S., Shenderov, K., Huang, N.N., Kabat, J., Abu-Asab, M., Fitzgerald, K.A., Sher, A., and Kehrl, J.H. (2012). Activation of autophagy by inflammatory signals limits IL-1beta production by targeting ubiquitinated inflammasomes for destruction. Nature immunology *13*, 255-263.

Shi, J., Zhao, Y., Wang, K., Shi, X., Wang, Y., Huang, H., Zhuang, Y., Cai, T., Wang, F., and Shao, F. (2015). Cleavage of GSDMD by inflammatory caspases determines pyroptotic cell death. Nature *526*, 660-665.

Shimada, K., Crother, T.R., Karlin, J., Dagvadorj, J., Chiba, N., Chen, S., Ramanujan, V.K., Wolf, A.J., Vergnes, L., Ojcius, D.M.*, et al.* (2012). Oxidized mitochondrial DNA activates the NLRP3 inflammasome during apoptosis. Immunity *36*, 401-414.

Smirnova, E., Griparic, L., Shurland, D.L., and van der Bliek, A.M. (2001). Dynamin-related protein Drp1 is required for mitochondrial division in mammalian cells. Molecular biology of the cell *12*, 2245-2256.

Stacpoole, P.W. (2012). The pyruvate dehydrogenase complex as a therapeutic target for age-related diseases. Aging cell *11*, 371-377.

Sun, W., Xie, Z., Liu, Y., Zhao, D., Wu, Z., Zhang, D., Lv, H., Tang, S., Jin, N., Jiang, H.*, et al.* (2015). JX06 Selectively Inhibits Pyruvate Dehydrogenase Kinase PDK1 by a Covalent Cysteine Modification. Cancer research *75*, 4923-4936.

Swain, A., Bambouskova, M., Kim, H., Andhey, P.S., Duncan, D., Auclair, K., Chubukov, V., Simons, D.M., Roddy, T.P., Stewart, K.M.*, et al.* (2020). Comparative evaluation of itaconate and its derivatives reveals divergent inflammasome and type I interferon regulation in macrophages. Nature metabolism *2*, 594-602.

Tannahill, G.M., Curtis, A.M., Adamik, J., Palsson-McDermott, E.M., McGettrick, A.F., Goel, G., Frezza, C., Bernard, N.J., Kelly, B., Foley, N.H.*, et al.* (2013). Succinate is an inflammatory signal that induces IL-1beta through HIF-1alpha. Nature *496*, 238-242.

Wang, Z., Zhao, Q., Nie, Y., Yu, Y., Misra, B.B., Zabalawi, M., Chou, J.W., Key, C.C., Molina, A.J., Quinn, M.A.*, et al.* (2020). Solute Carrier Family 37 Member 2 (SLC37A2) Negatively Regulates Murine Macrophage Inflammation by Controlling Glycolysis. iScience *23*, 101125.

Wu, C., Lu, W., Zhang, Y., Zhang, G., Shi, X., Hisada, Y., Grover, S.P., Zhang, X., Li, L., Xiang, B.*, et al.* (2019). Inflammasome Activation Triggers Blood Clotting and Host Death through Pyroptosis. Immunity *50*, 1401-1411.

Wu, J., Zhao, Y., Park, Y.K., Lee, J.Y., Gao, L., Zhao, J., and Wang, L. (2018). Loss of PDK4 switches the hepatic NF-κB/TNF pathway from pro-survival to pro-apoptosis. Hepatology (Baltimore, Md) *68*, 1111-1124.

Xian, H., Liu, Y., Rundberg Nilsson, A., Gatchalian, R., Crother, T.R., Tourtellotte, W.G., Zhang, Y., Aleman-Muench, G.R., Lewis, G., Chen, W.*, et al.* (2021). Metformin inhibition of mitochondrial ATP and DNA synthesis abrogates NLRP3 inflammasome activation and pulmonary inflammation. Immunity *54*, 1463-1477.

Zhang, M., Kenny, S.J., Ge, L., Xu, K., and Schekman, R. (2015). Translocation of interleukin-1β into a vesicle intermediate in autophagy-mediated secretion. eLife *4*.

Zhong, Z., Liang, S., Sanchez-Lopez, E., He, F., Shalapour, S., Lin, X.J., Wong, J., Ding, S., Seki, E., Schnabl, B.*, et al.* (2018). New mitochondrial DNA synthesis enables NLRP3 inflammasome activation. Nature.

Zhou, R., Yazdi, A.S., Menu, P., and Tschopp, J. (2011). A role for mitochondria in NLRP3 inflammasome activation. Nature *469*, 221-225.

Zhu, X., Lee, J.Y., Timmins, J.M., Brown, J.M., Boudyguina, E., Mulya, A., Gebre, A.K., Willingham, M.C., Hiltbold, E.M., Mishra, N.*, et al.* (2008). Increased cellular free cholesterol in macrophage-specific Abca1 knock-out mice enhances pro-inflammatory response of macrophages. The Journal of biological chemistry *283*, 22930-22941.

Zhu, X., Long, D., Zabalawi, M., Ingram, B., Yoza, B.K., Stacpoole, P.W., and McCall, C.E. (2020). Stimulating pyruvate dehydrogenase complex reduces itaconate levels and enhances TCA cycle anabolic bioenergetics in acutely inflamed monocytes. Journal of leukocyte biology *107*, 467-484.

# Figure 1

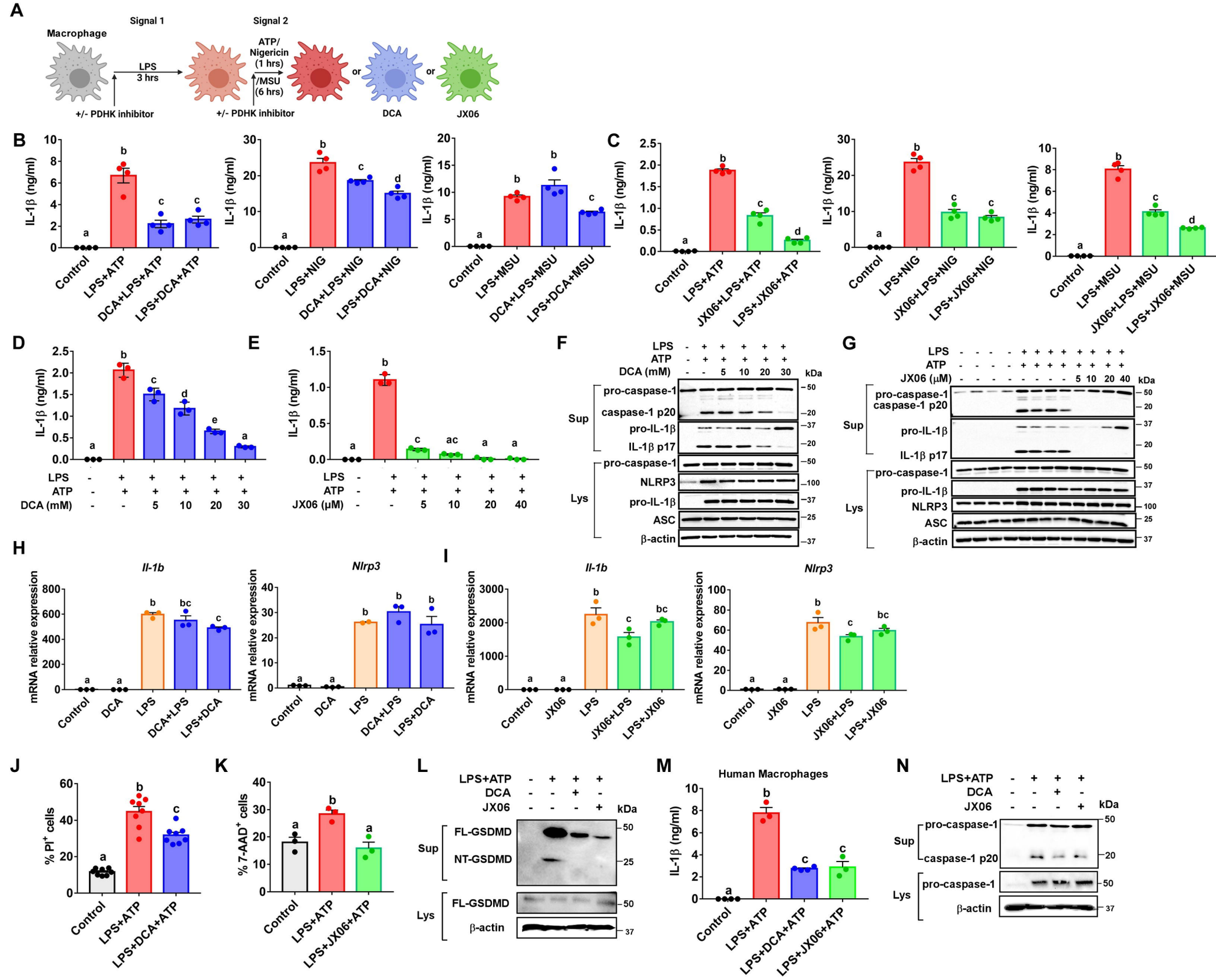
A
Signal 1
Signal 2
Macrophage
LPS
3 hrs
ATP/
Nigericin
(1 hrs)
/MSU
(6 hrs)
or
or
+/- PDHK inhibitor
+/- PDHK inhibitor
DCA
JX06
B
IL-1β (ng/ml)
Control
LPS+ATP
DCA+LPS+ATP
LPS+DCA+ATP
LPS+NIG
DCA+LPS+NIG
LPS+DCA+NIG
LPS+MSU
DCA+LPS+MSU
LPS+DCA+MSU
C
JX06+LPS+ATP
LPS+JX06+ATP
JX06+LPS+NIG
LPS+JX06+NIG
JX06+LPS+MSU
LPS+JX06+MSU
D
LPS
ATP
DCA (mM)
E
JX06 (μM)
F
Sup
Lys
pro-caspase-1
caspase-1 p20
pro-IL-1β
IL-1β p17
NLRP3
ASC
β-actin
kDa
G
H
Il-1b
Nlrp3
mRNA relative expression
DCA
LPS
LPS+DCA
I
JX06
JX06+LPS
LPS+JX06
J
% PI+ cells
K
% 7-AAD+ cells
L
LPS+ATP
FL-GSDMD
NT-GSDMD
M
Human Macrophages
N

# Figure 2

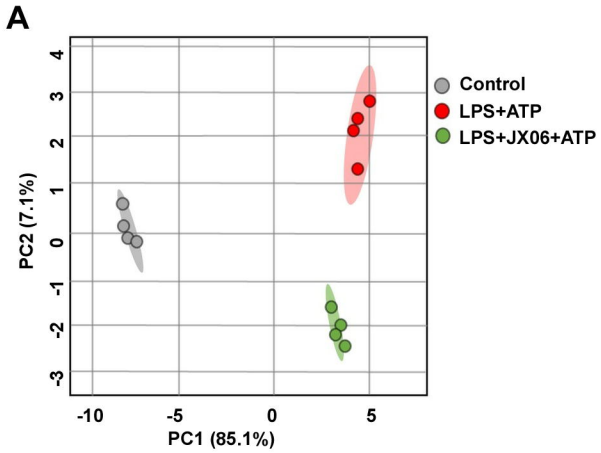


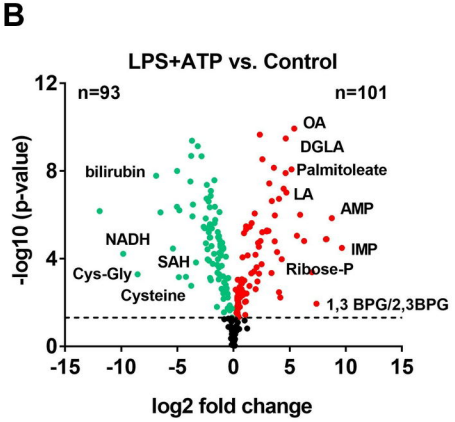


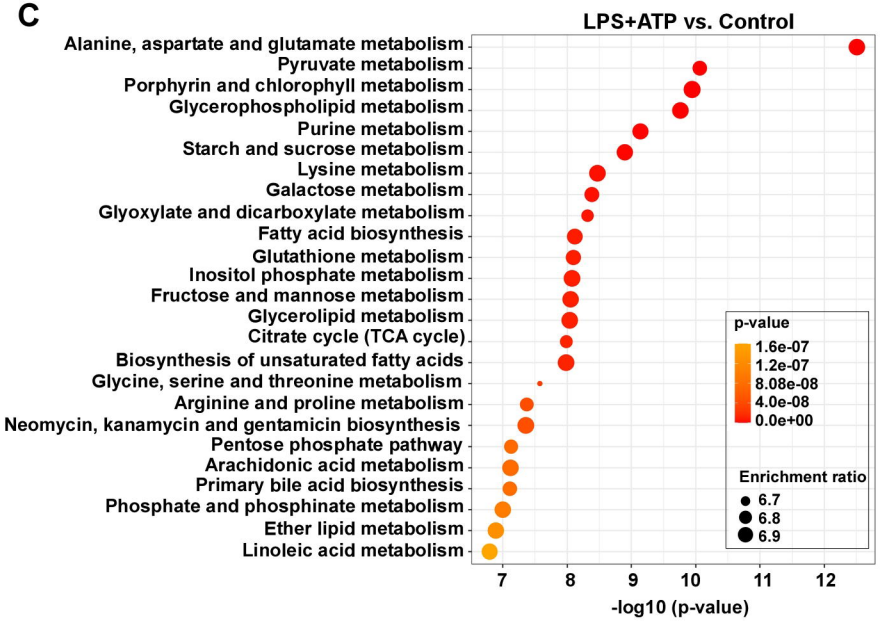


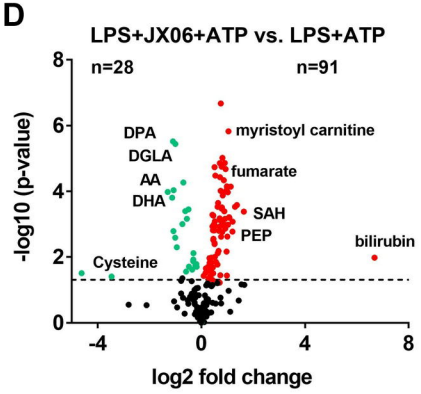


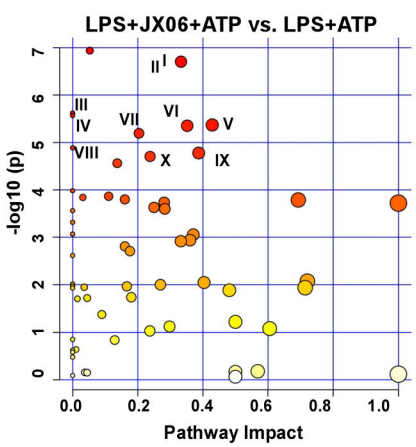


| Number | Pathway name | -log (p) | Impact |
|---|---|---|---|
| I | Porphyrin and chlorophyll metabolism | 6.938 | 0.05288 |
| II | Arachidonic acid metabolism | 6.7044 | 0.33292 |
| III | Fatty acid degradation | 5.6221 | 0.0 |
| IV | Biosynthesis of unsaturated fatty acids | 5.5677 | 0.0 |
| V | Nicotinate and nicotinamide metabolism | 5.3689 | 0.42895 |
| VI | Citrate cycle (TCA cycle) | 5.3531 | 0.35197 |
| VII | Glycerophospholipid metabolism | 5.193 | 0.20382 |
| VIII | Either lipid metabolism | 4.8866 | 0.0 |
| IX | Pentose phosphate pathway | 4.7765 | 0.38726 |
| X | Pyruvate metabolism | 4.7044 | 0.23794 |

# Figure 3

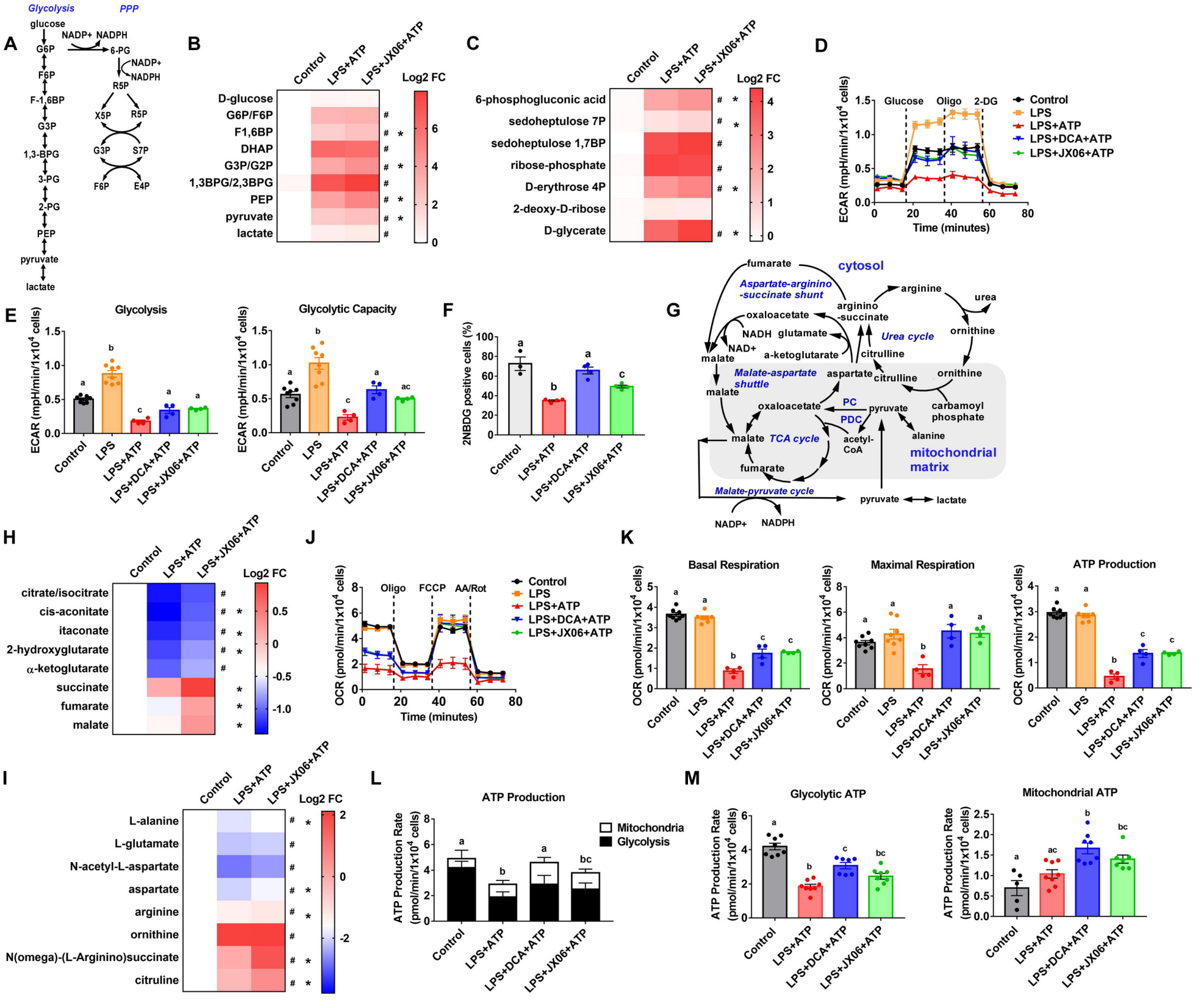
A
Glycolysis
PPP
glucose
G6P
F6P
F-1,6BP
G3P
1,3-BPG
3-PG
2-PG
PEP
pyruvate
lactate
NADP+ NADPH
6-PG
NADP+
NADPH
R5P
X5P
R5P
G3P
S7P
F6P
E4P
B
Control
LPS+ATP
LPS+JX06+ATP
Log2 FC
D-glucose
G6P/F6P
F1,6BP
DHAP
G3P/G2P
1,3BPG/2,3BPG
PEP
pyruvate
lactate
C
6-phosphogluconic acid
sedoheptulose 7P
sedoheptulose 1,7BP
ribose-phosphate
D-erythrose 4P
2-deoxy-D-ribose
D-glycerate
D
Glucose
Oligo
2-DG
Control
LPS
LPS+ATP
LPS+DCA+ATP
LPS+JX06+ATP
ECAR (mpH/min/1x10^4 cells)
Time (minutes)
E
Glycolysis
Glycolytic Capacity
F
2NBDG positive cells (%)
G
cytosol
fumarate
Aspartate-arginino -succinate shunt
arginine
urea
arginino -succinate
oxaloacetate
NADH
glutamate
Urea cycle
ornithine
NAD+
a-ketoglutarate
citrulline
malate
Malate-aspartate shuttle
aspartate
citrulline
ornithine
malate
oxaloacetate
PC
pyruvate
carbamoyl phosphate
PDC
malate
TCA cycle
acetyl-CoA
alanine
mitochondrial matrix
fumarate
Malate-pyruvate cycle
pyruvate
lactate
NADP+
NADPH
H
citrate/isocitrate
cis-aconitate
itaconate
2-hydroxyglutarate
α-ketoglutarate
succinate
fumarate
malate
J
Oligo
FCCP
AA/Rot
OCR (pmol/min/1x10^4 cells)
Time (minutes)
K
Basal Respiration
Maximal Respiration
ATP Production
I
L-alanine
L-glutamate
N-acetyl-L-aspartate
aspartate
arginine
ornithine
N(omega)-(L-Arginino)succinate
citruline
L
ATP Production
Mitochondria
Glycolysis
ATP Production Rate (pmol/min/1x10^4 cells)
M
Glycolytic ATP
Mitochondrial ATP

# Figure 4

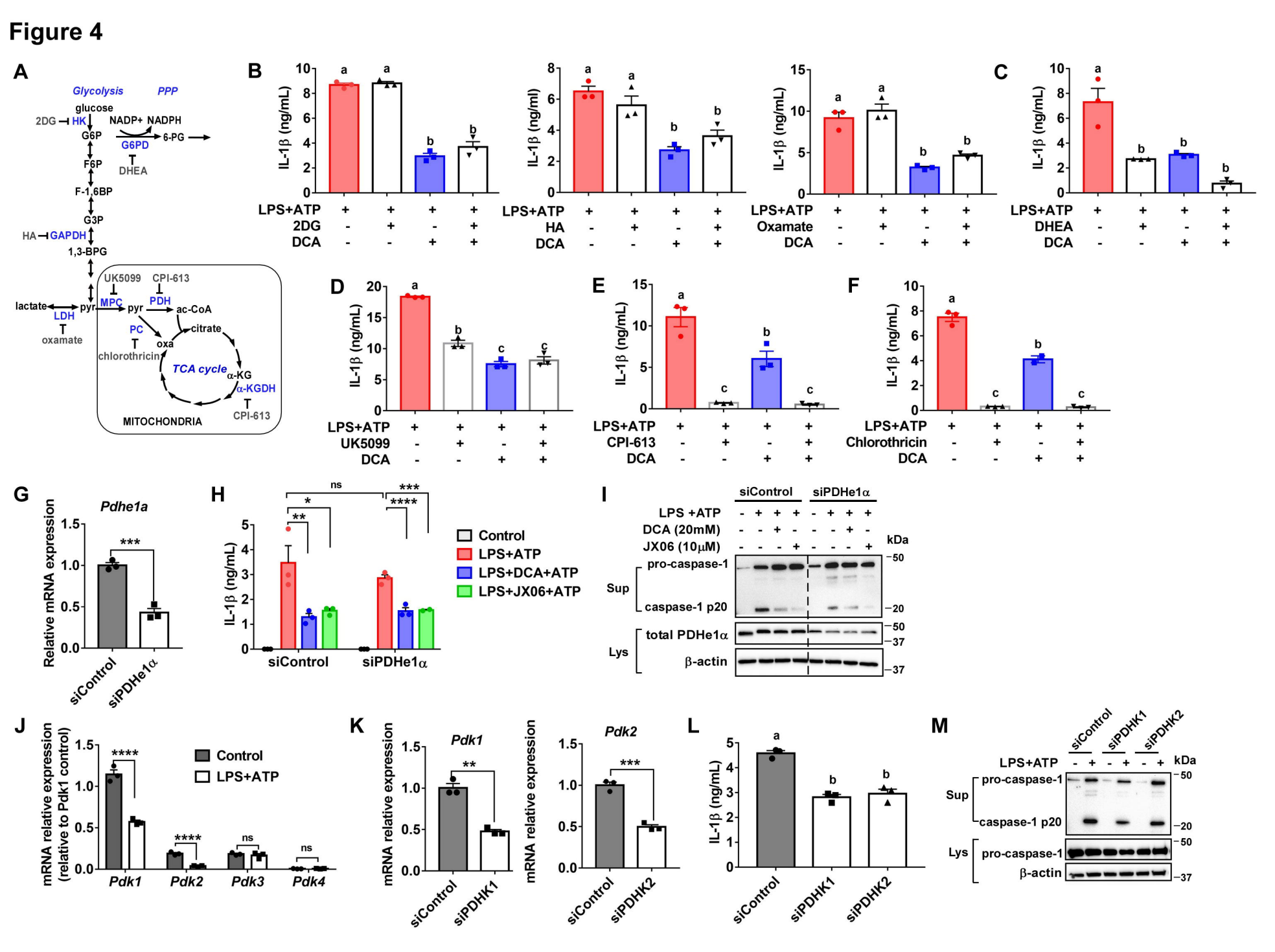
A
Glycolysis
PPP
glucose
2DG
HK
NADP+ NADPH
G6P
6-PG
G6PD
DHEA
F6P
F-1,6BP
G3P
HA
GAPDH
1,3-BPG
UK5099
CPI-613
lactate
pyr
MPC
PDH
ac-CoA
LDH
oxamate
PC
citrate
oxa
chlorothricin
TCA cycle
α-KG
α-KGDH
CPI-613
MITOCHONDRIA
B
IL-1β (ng/mL)
LPS+ATP
2DG
DCA
IL-1β (ng/ml)
HA
Oxamate
C
DHEA
D
UK5099
E
CPI-613
F
Chlorothricin
G
Pdhe1a
Relative mRNA expression
siControl
siPDHe1α
H
ns
Control
LPS+ATP
LPS+DCA+ATP
LPS+JX06+ATP
I
siControl
siPDHe1α
LPS +ATP
DCA (20mM)
JX06 (10μM)
kDa
pro-caspase-1
Sup
caspase-1 p20
total PDHe1α
Lys
β-actin
J
mRNA relative expression (relative to Pdk1 control)
Control
LPS+ATP
Pdk1
Pdk2
Pdk3
Pdk4
K
mRNA relative expression
siPDHK1
siPDHK2
L
M
siPDHK1
siPDHK2

# Figure 5

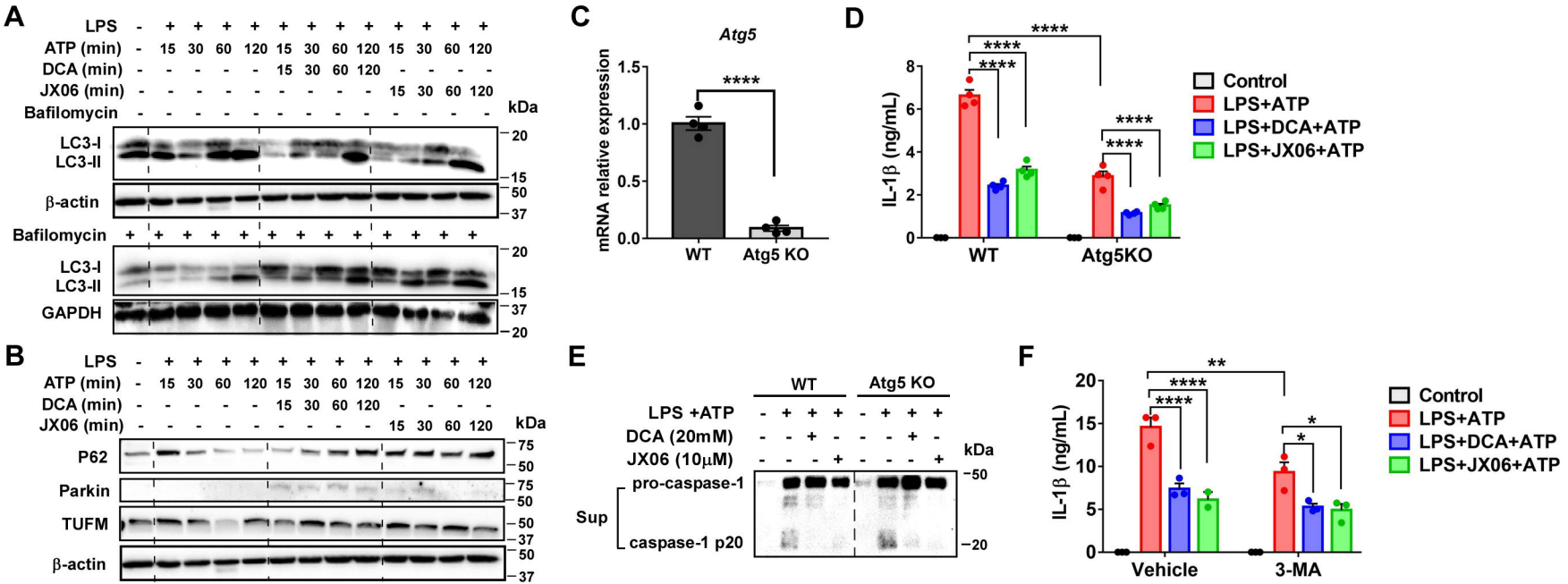
A
LPS
ATP (min)
DCA (min)
JX06 (min)
Bafilomycin
kDa
LC3-I
LC3-II
β-actin
GAPDH
B
P62
Parkin
TUFM
C
Atg5
mRNA relative expression
WT
Atg5 KO
D
IL-1β (ng/mL)
Control
LPS+ATP
LPS+DCA+ATP
LPS+JX06+ATP
Atg5KO
E
LPS +ATP
DCA (20mM)
JX06 (10μM)
pro-caspase-1
caspase-1 p20
Sup
F
Vehicle
3-MA

# Figure 6

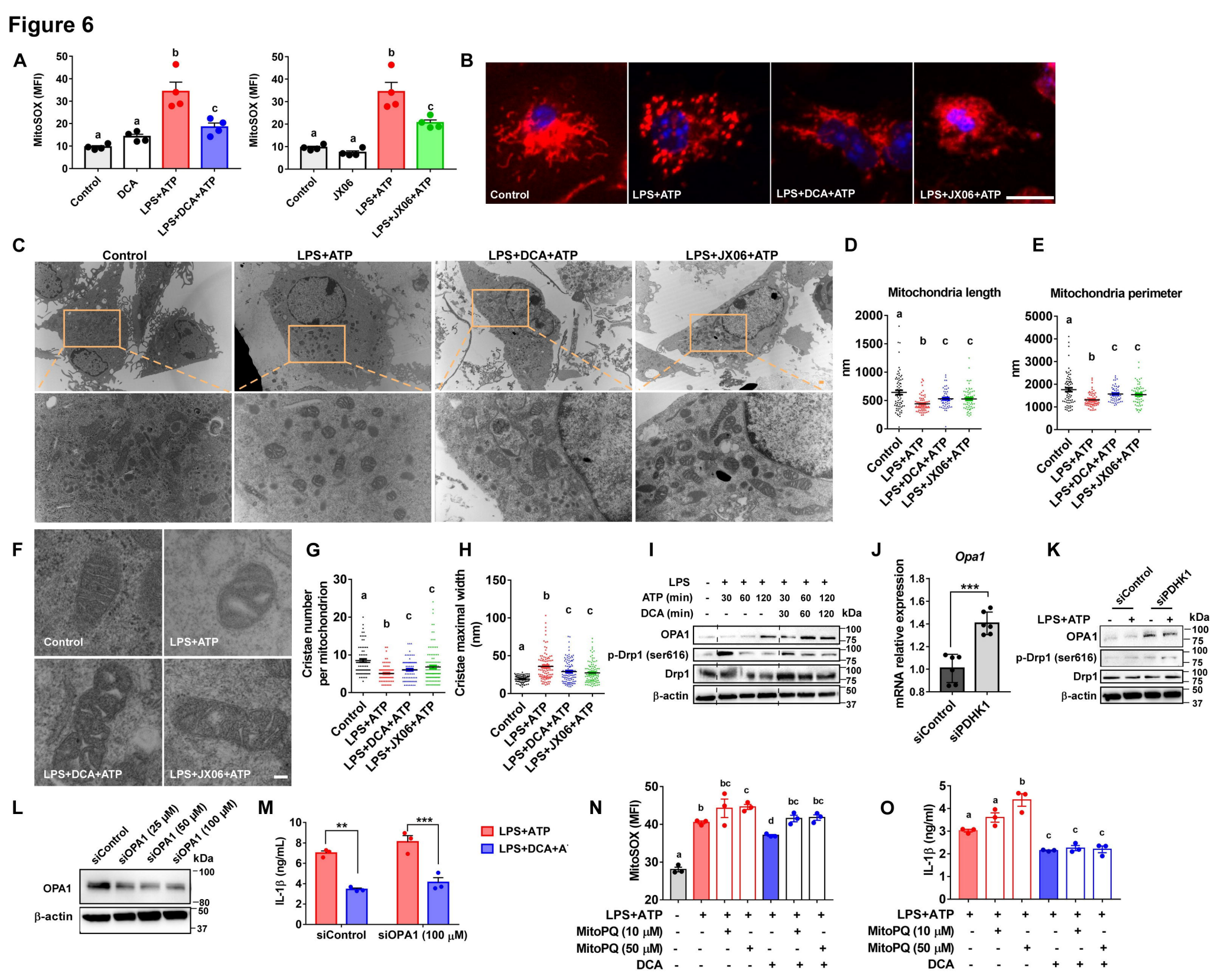
A
MitoSOX (MFI)
Control
DCA
LPS+ATP
LPS+DCA+ATP
JX06
LPS+JX06+ATP
B
Control
LPS+ATP
LPS+DCA+ATP
LPS+JX06+ATP
C
Control
LPS+ATP
LPS+DCA+ATP
LPS+JX06+ATP
D
Mitochondria length
nm
E
Mitochondria perimeter
nm
F
Control
LPS+ATP
LPS+DCA+ATP
LPS+JX06+ATP
G
Cristae number per mitochondrion
H
Cristae maximal width (nm)
I
LPS
ATP (min)
DCA (min)
kDa
OPA1
p-Drp1 (ser616)
Drp1
β-actin
J
Opa1
mRNA relative expression
siControl
siPDHK1
K
siControl
siPDHK1
LPS+ATP
OPA1
p-Drp1 (ser616)
Drp1
β-actin
L
siControl
siOPA1 (25 μM)
siOPA1 (50 μM)
siOPA1 (100 μM)
kDa
OPA1
β-actin
M
IL-1β (ng/mL)
siControl
siOPA1 (100 μM)
LPS+ATP
LPS+DCA+A
N
MitoSOX (MFI)
LPS+ATP
MitoPQ (10 μM)
MitoPQ (50 μM)
DCA
O
IL-1β (ng/ml)
LPS+ATP
MitoPQ (10 μM)
MitoPQ (50 μM)
DCA

# Figure 7

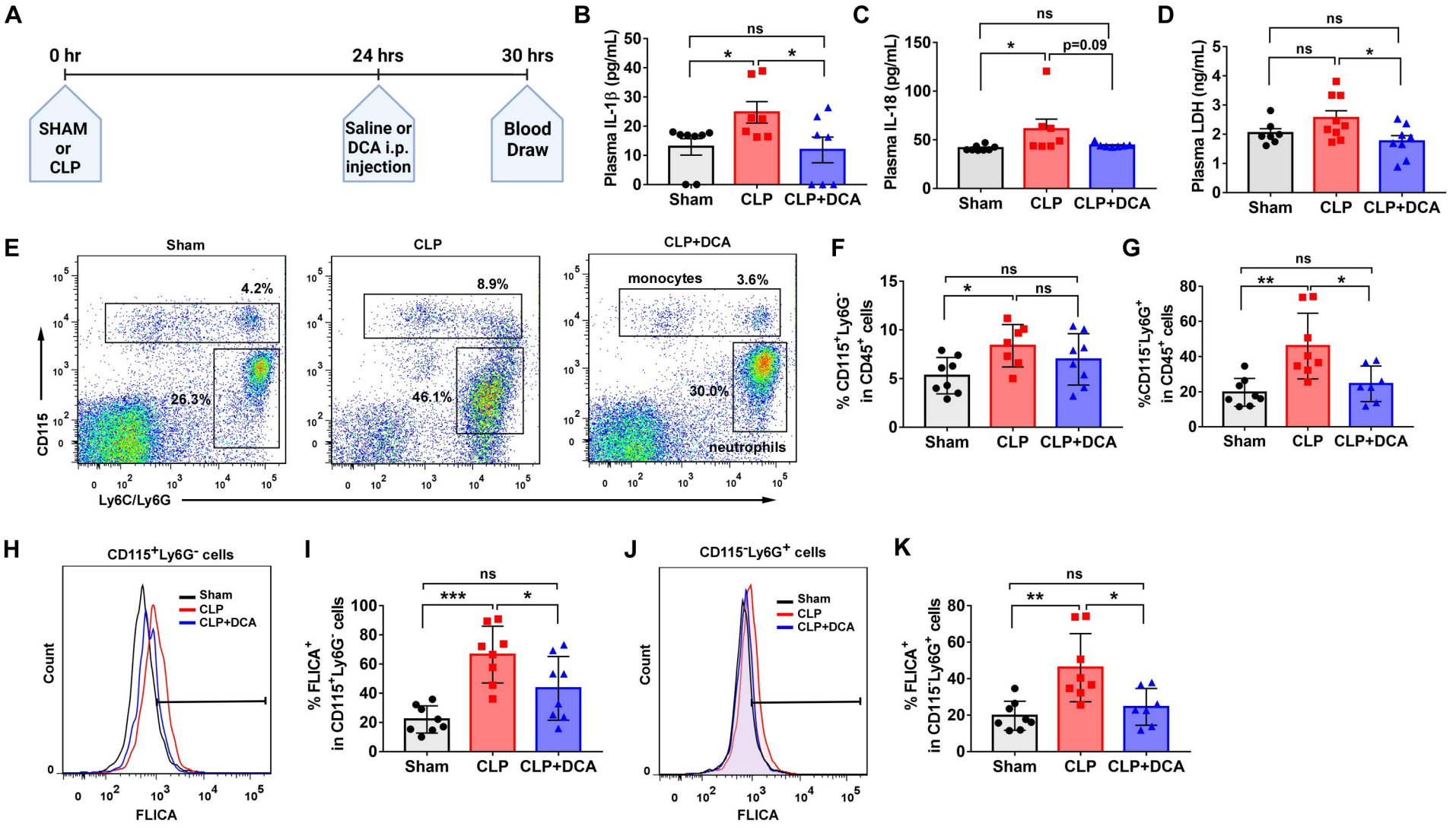
A
0 hr
24 hrs
30 hrs
SHAM or CLP
Saline or DCA i.p. injection
Blood Draw
B
Plasma IL-1β (pg/mL)
ns
*
*
Sham
CLP
CLP+DCA
C
Plasma IL-18 (pg/mL)
ns
*
p=0.09
D
Plasma LDH (ng/mL)
ns
ns
*
E
Sham
CLP
CLP+DCA
4.2%
26.3%
8.9%
46.1%
monocytes
3.6%
30.0%
neutrophils
CD115
Ly6C/Ly6G
F
% CD115+Ly6G- in CD45+ cells
G
%CD115-Ly6G+ in CD45+ cells
H
CD115+Ly6G- cells
Sham
CLP
CLP+DCA
Count
FLICA
I
% FLICA+ in CD115+Ly6G- cells
***
J
CD115-Ly6G+ cells
K
% FLICA+ in CD115-Ly6G+ cells
**